

WIMPs in Dilatonic Einstein Gauss-Bonnet Cosmology

**Anirban Biswas,^{a,b} Arpan Kar,^b Bum-Hoon Lee,^{b,c} Hocheol Lee,^{b,c} Wonwoo Lee,^b
Stefano Scopel,^{b,c} Liliana Velasco-Sevilla,^{b,c} Lu Yin^{b,d}**

^a*Department of Physics & Lab of Dark Universe, Yonsei University, Seoul 03722, Republic of Korea*

^b*Center for Quantum Spacetime, Sogang University, Seoul 121-742, South Korea*

^c*Department of Physics, Sogang University, Seoul 121-742, South Korea*

^d*Asia Pacific Center for Theoretical Physics (APCTP) San 31, Hyoja-dong, Nam-gu, Pohang 790-784, South Korea*

E-mail: anirban.biswas.sinp@gmail.com, arpankarphys@gmail.com,
bhl@sogang.ac.kr, insaying@sogang.ac.kr, warrrior@sogang.ac.kr,
scopel@sogang.ac.kr, liliana.velascosevilla@gmail.com,
lu.yin@apctp.org

ABSTRACT: We use the Weakly Interacting Massive Particle (WIMP) thermal decoupling scenario to probe Cosmologies in dilatonic Einstein Gauss-Bonnet (dEGB) gravity, where the Gauss-Bonnet term is non-minimally coupled to a scalar field with vanishing potential. We put constraints on the model parameters when the ensuing modified cosmological scenario drives the WIMP annihilation cross section beyond the present bounds from DM indirect detection searches. In our analysis we assumed WIMPs that annihilate to Standard Model particles through an s-wave process. For the class of solutions that comply with WIMP indirect detection bounds, we find that dEGB typically plays a mitigating role on the scalar field dynamics at high temperature, slowing down the speed of its evolution and reducing the enhancement of the Hubble constant compared to its standard value. For such solutions, we observe that the corresponding boundary conditions at high temperature correspond asymptotically to a vanishing deceleration parameter q , so that the effect of dEGB is to add an accelerating term that exactly cancels the deceleration predicted by General Relativity. The bounds from WIMP indirect detection are nicely complementary to late-time constraints from compact binary mergers. This suggests that it could be interesting to use other Early Cosmology processes to probe the dEGB scenario.

Contents

1	Introduction	1
2	Summary of Gauss-Bonnet theory	3
3	WIMP thermal relic density and indirect detection bounds	6
3.1	WIMP relic density	6
3.2	Indirect detection bounds on WIMP annihilation	8
4	Results	9
4.1	Numerical solutions of Friedmann equations	9
4.2	Constraints on the dEGB scenario	16
4.2.1	Black hole and neutron star binaries	16
4.2.2	WIMP indirect detection	19
5	Conclusions	22
A	Comments on the semi-analytical solutions of the Friedmann equations	23
A.1	Equation of state of the dEGB term at temperatures close to Big Bang Nucleosynthesis	23
A.2	Back-reaction on the scalar field evolution from the change of sign of the deceleration parameter	24
A.3	Equation of state at high temperature for subdominant kination energy	25

1 Introduction

The difficulty to fit General Relativity (GR) with the other fundamental interactions of the Standard Model of Particle Physics (SM) and the failure of the latter to stabilize at the weak scale (naturalness problem) imply that in spite of their great effectiveness to describe the observed Universe both theories are believed to be incomplete. Cosmology and Astrophysics represent excellent testbeds to probe possible extensions of both GR and the SM.

Indeed, the discovery of Gravitational Waves (GW) and the direct measurement of merger events of compact binaries has opened up a new era of precision tests of GR that complement constraints from Cosmology [1, 2] and from laboratory and planetary observations [3]. In this context, a particularly effective approach to probe extensions of GR using observational data is the use of effective models.

Among effective modifications of GR, higher curvature terms are expected to appear in extensions of Einstein Gravity such as string theory and to become important in the early

Universe. In particular, Horndeski’s theory is the most general scalar-tensor theory having equations of motion with second-order time derivatives in four-dimensional spacetime [4], in which the theory does not have a ghost state [5]. Examples of Horndeski’s theory include additional scalar fields (quintessence [6–11], $f(\phi)R$ gravity [12]) and/or curvature terms ($f(R)$ gravity [13]). At the level of the equation of motion [4, 5] the simplest example of Horndeski’s theory containing higher-curvature terms is the dilaton-Einstein-Gauss-Bonnet (dEGB) theory, obtained by adding a specific quadratic combination of the curvature non-minimally coupled to a scalar field [14, 15] (without such non-minimal coupling the Gauss-Bonnet term becomes a topological invariant that does not affect the dynamics). The dEGB theory has been extensively studied in various realizations [14–33]. In particular, constraints on the dEGB scenario have already been derived using the observed GW signal from Black Hole (BH-BH) or Black Hole-neutron star (BH-NS) merger events [34–38].

At the temperature $T_{\text{BBN}} \simeq 1$ MeV, Big Bang Nucleosynthesis (BBN) is the earliest process in Cosmology providing a successful confirmation of both GR and the SM, strongly constraining any departure from Standard Cosmology [39, 40]. On the other hand, although we have no direct probe of the Universe expansion rate, composition or reheating temperature before BBN, an understanding of the present Universe cannot dispense from encompassing Inflation, Dark Matter (DM) and Baryon asymmetry. All events that take place at $T > T_{\text{BBN}}$ can be used to shed light on physics beyond GR and the SM. An explicit example of such approach is, for instance, to identify the dilaton scalar field with the inflaton and to work out observational constraints on dEGB inflation [19, 20, 41].

Specifically, in the present paper we wish to use the physics of Weakly Interacting Massive Particles (WIMPs) decoupling to probe dEGB Cosmologies (for examples of analyses where the WIMP relic density has been studied within the context of modified Cosmologies see [42–49]). WIMPs are the most popular candidates to provide the Cold Dark Matter (CDM) which is supposed to account for about 25% of the observed energy density of the Universe and explain Galaxy formation. In particular, CDM is one of the most important open issues in modern physics, since the SM provides no candidate for it and as a consequence it requires to introduce exotic physics. WIMPs are expected to have a mass m_χ in the GeV-TeV range and provide the correct relic abundance $\Omega_\chi h^2 \simeq 0.12$ through thermal decoupling with the relativistic plasma for an annihilation cross section with SM particles $\langle\sigma v\rangle_f \simeq 3 \times 10^{-26} \text{ cm}^3\text{s}^{-1}$, with the standard assumption that the energy density of the Universe is dominated by radiation and the Hubble constant scales with the temperature T as $H(T) \sim T^2$ at the freeze-out temperature $T_f \simeq m_\chi/20 \simeq 50 \text{ MeV} \sim 50 \text{ GeV}^1$.

Experimental bounds on such scenarios can be obtained by exploiting the fact that the value of $\langle\sigma v\rangle_f$ that corresponds to the correct CDM relic abundance becomes larger for Cosmologies that enhance $H(T)$ at the time of the WIMP freeze-out, eventually driving the WIMP annihilation rate in our Galaxy today beyond the observational limits on photons, electrons (positrons), (anti)protons and (anti)neutrinos fluxes. For instance, this approach has already been used in the literature to constrain scenarios where $H(T)$ is modified using

¹As usual, $\Omega_\chi = \rho_\chi/\rho_c$ with ρ_χ the WIMP number density, $\rho_c = 1.8791 h^2 \times 10^{-29} \text{ g cm}^{-3}$ the critical density of the Universe and $h = H_0/100 \text{ km s}^{-1} \text{ Mpc}^{-1}$ with H_0 the Hubble parameter at present time.

simple phenomenological parameterizations [50, 51]. In the following, we will apply the same strategy to constrain the dEGB scenario. As we will show, due to the scalar field evolution, dEGB presents a high degree of non linearity that implies a more complex phenomenology compared to simplified phenomenological realizations. In particular, this will require to solve the coupled differential equations that drive the WIMP freeze-out process and the scalar field evolution numerically. Interestingly, we will find a degree of complementarity between Late Universe constraints and this specific class of Early Cosmology bounds. This suggests that it could be interesting to further pursue such approach using other Early Cosmology processes, such as for instance thermal leptogenesis, that would allow to probe dEGB at even higher temperatures [52, 53].

The paper is organized as follows. In Section 2 we outline the dEGB scenario of modified gravity and fix our notations. Section 3 is devoted to a summary of the physics that drives the WIMP thermal relic density (Section 3.1) and the present indirect signals in our Galaxy that can be used to constrain WIMPs (Section 3.2). Our quantitative results are contained in Section 4. Specifically, the numerical solution of Friedmann equations in dEGB Cosmology is discussed in Section 4.1, the Late Universe constraints from BH-BH and BH-NS merger events are summarized for convenience in Section 4.2.1, while our main results, i.e. the bounds on the dEGB parameter space from WIMP indirect detection, are discussed in Section 4.2.2 and combined with those from Section 4.2.1. Our Conclusions are provided in Section 5, while in Appendix A we provide a qualitative insight on the class of solutions that are obtained numerically by making use of semi-analytical expressions.

2 Summary of Gauss-Bonnet theory

In this Section we briefly summarize the dEGB scenario and fix our notations (more details can be found in [17, 20, 24, 28–31]). The action is given by:

$$S = \int_{\mathcal{M}} \sqrt{-g} d^4x \left[\frac{R}{2\kappa} - \frac{1}{2} \nabla_\mu \phi \nabla^\mu \phi - V(\phi) + f(\phi) R_{\text{GB}}^2 + \mathcal{L}_m^{\text{rad}} \right], \quad (2.1)$$

where $\kappa \equiv 8\pi G = 1/M_{PL}^2$ (with M_{PL} the reduced Planck mass), R denotes the scalar curvature of the spacetime \mathcal{M} , $R_{\text{GB}}^2 = R^2 - 4R_{\mu\nu}R^{\mu\nu} + R_{\mu\nu\rho\sigma}R^{\mu\nu\rho\sigma}$ is the Gauss-Bonnet term and $\mathcal{L}_m^{\text{rad}}$ describes the interactions of radiation and matter fields.

The coupling between the scalar field and the Gauss-Bonnet term is driven by a function of the scalar field $f(\phi)$. If it is chosen to be a constant, the Gauss-Bonnet term doesn't contribute to the equations of motion being a surface term. The theory can then be reduced to a quintessence model [6–11]. The coupling function is in principle arbitrary. An exponential form arises within theories where gravity is coupled to the dilaton [17, 25, 29, 31]. A power law has also been adopted in the literature [26, 27] (the two forms are connected by a field redefinition). In the present analysis, we will then adopt the following dEGB realization:

$$f(\phi) = \alpha e^{\gamma\phi}. \quad (2.2)$$

Notice that in string theory the natural sign of the α coefficient is positive [54]. In Refs. [20, 29, 31] it was shown that for both signs of α black-hole solutions can be found. In our phenomenological analysis we will adopt both signs.

By varying the action one obtains the equation of motion of the scalar field:

$$\square\phi - V' + f'R_{\text{GB}}^2 = 0, \quad (2.3)$$

and Einstein's equations:

$$R_{\mu\nu} - \frac{1}{2}g_{\mu\nu}R = \kappa \left(T_{\mu\nu}^\phi + T_{\mu\nu}^{\text{GB}} + T_{\mu\nu}^{\text{rad}} \right) \equiv \kappa T_{\mu\nu}^{\text{tot}}, \quad (2.4)$$

where $\square = \nabla_\mu \nabla^\mu$, $V' = \partial V / \partial \phi$ and $f' = \partial f / \partial \phi$. We moved all the additional terms to the right hand side so that it is in the familiar form of the Einstein Equation.

The total energy-momentum tensor $T_{\mu\nu}^{\text{tot}}$ consists of three terms: $T_{\mu\nu}^\phi$ arises from the scalar field action:

$$T_{\mu\nu}^\phi = \nabla_\mu \phi \nabla_\nu \phi - \left(\frac{1}{2} \nabla_\rho \phi \nabla^\rho \phi + V \right) g_{\mu\nu}, \quad (2.5)$$

$T_{\mu\nu}^{\text{GB}}$ from the formal contribution of the dEGB term:

$$\begin{aligned} T_{\mu\nu}^{\text{GB}} = & 4 [R \nabla_\mu \nabla_\nu f(\phi) - g_{\mu\nu} R \square f(\phi)] - 8 [R_\nu{}^\rho \nabla_\rho \nabla_\mu f(\phi) + R_\mu{}^\rho \nabla_\rho \nabla_\nu f(\phi) \\ & - R_{\mu\nu} \square f(\phi) - g_{\mu\nu} R^{\rho\sigma} \nabla_\rho \nabla_\sigma f(\phi) + R_{\mu\rho\nu\sigma} \nabla^\rho \nabla^\sigma f(\phi)], \end{aligned} \quad (2.6)$$

while $T_{\mu\nu}^{\text{rad}}$ is the usual energy-momentum tensor for radiation:

$$T_{\mu\nu}^{\text{rad}} = -2 \frac{\delta \mathcal{L}_m^{\text{rad}}}{\delta g^{\mu\nu}} + \mathcal{L}_m^{\text{rad}} g_{\mu\nu}. \quad (2.7)$$

We take the spatially flat Friedmann-Lemaître-Robertson-Walker (FLRW) metric:

$$ds^2 = -dt^2 + a^2(t) \delta_{ij} dx^i dx^j, \quad (2.8)$$

that implies that the scalar field depends only on time, $\phi = \phi(t)$. The energy density and the pressure can be obtained from the energy-momentum tensor as $-\rho_I = T_I^0{}_0$ and $T_I^i{}_j = p_I \delta^i{}_j$, where $I = \{\phi, \text{GB}, \text{rad}\}$. Specifically, the energy density and pressure for the scalar are

$$\rho_\phi = \frac{1}{2} \dot{\phi}^2 + V(\phi), \quad p_\phi = \frac{1}{2} \dot{\phi}^2 - V(\phi), \quad (2.9)$$

while the corresponding formal quantities from the Gauss-Bonnet term are:

$$\rho_{\text{GB}} = -24 \dot{f} H^3 = -24 f' \dot{\phi} H^3 = -24 \alpha \gamma e^{\gamma \phi} \dot{\phi} H^3. \quad (2.10)$$

$$\begin{aligned} p_{\text{GB}} = & 8 \left(f'' \dot{\phi}^2 + f' \ddot{\phi} \right) H^2 + 16 f' \dot{\phi} H (\dot{H} + H^2) \\ = & 8 \frac{d(\dot{f} H^2)}{dt} + 16 \dot{f} H^3 = 8 \frac{d(\dot{f} H^2)}{dt} - \frac{2}{3} \rho_{\text{GB}}. \end{aligned} \quad (2.11)$$

Here, $H(t) = \frac{\dot{a}(t)}{a(t)}$ is the Hubble parameter, a the scale factor, $\dot{f} = f' \dot{\phi}$ and $\ddot{f} = f'' \dot{\phi}^2 + f' \ddot{\phi}$. The radiation energy density ρ_{rad} and pressure p_{rad} from Eq. (2.7) are taking contribution

from all relativistic species satisfying the equation of state $p_{\text{rad}} = \frac{1}{3}\rho_{\text{rad}}$. The energy density ρ_{rad} at temperature T is given by $\rho_{\text{rad}} = \frac{\pi^2}{30} g_* T^4$ with g_* the number of effective relativistic degrees of freedom in equilibrium with the thermal bath. The total energy-momentum tensor satisfies the continuity equation. Specifically, radiation satisfies:

$$\dot{\rho}_{\text{rad}} + 3H(\rho_{\text{rad}} + p_{\text{rad}}) = 0. \quad (2.12)$$

Similarly, the sum of the scalar and the Gauss-Bonnet contributions can be shown to satisfy:

$$\dot{\rho}_{\{\phi+\text{GB}\}} + 3H(\rho_{\{\phi+\text{GB}\}} + p_{\{\phi+\text{GB}\}}) = 0, \quad (2.13)$$

where the subscript $\{\phi + \text{GB}\}$ represents the sum of the contributions from the scalar field and the Gauss-Bonnet term, $\rho_{\{\phi+\text{GB}\}} \equiv \rho_{\phi} + \rho_{\text{GB}}$ and $p_{\{\phi+\text{GB}\}} \equiv p_{\phi} + p_{\text{GB}}$. However, the scalar and Gauss-Bonnet contributions don't satisfy the continuity equation separately. This is due to the interaction between the Gauss-Bonnet term and the scalar field. It is also worthwhile to mention that the signature of $\rho_{\{\phi+\text{GB}\}}$ and $p_{\{\phi+\text{GB}\}}$ is not necessarily positive.

The Friedmann equations can be written as [20]:

$$H^2 = \frac{\kappa}{3} (\rho_{\{\phi+\text{GB}\}} + \rho_{\text{rad}}) \equiv \frac{\kappa}{3} \rho_{\text{tot}}, \quad (2.14)$$

$$\dot{H} = -\frac{\kappa}{2} [(\rho_{\{\phi+\text{GB}\}} + p_{\{\phi+\text{GB}\}}) + (\rho_{\text{rad}} + p_{\text{rad}})] \equiv -\frac{\kappa}{2} (\rho_{\text{tot}} + p_{\text{tot}}), \quad (2.15)$$

$$\ddot{\phi} + 3H\dot{\phi} + V' - f'R_{\text{GB}}^2 = 0, \quad (2.16)$$

where ρ_{tot} and p_{tot} can be interpreted as the total energy density and the pressure of the Universe. The combination of Eqs. (2.14) and (2.15) gives the acceleration (deceleration) of expansion

$$\begin{aligned} \dot{H} + H^2 &= \frac{\ddot{a}}{a} \equiv -H^2 q \\ &= -\frac{\kappa}{6} ((\rho_{\{\phi+\text{GB}\}} + 3p_{\{\phi+\text{GB}\}}) + (\rho_{\text{rad}} + 3p_{\text{rad}})) \\ &= -\frac{\kappa}{6} \rho_{\text{tot}} (1 + 3w_{\text{tot}}) = -\frac{1}{2} H^2 (1 + 3w_{\text{tot}}), \end{aligned} \quad (2.17)$$

where:

$$q = -\frac{\ddot{a}a}{\dot{a}^2} = \frac{1}{2}(1 + 3w_{\text{tot}}), \quad (2.18)$$

is the deceleration parameter and $w_{\text{tot}} = \frac{p_{\text{tot}}}{\rho_{\text{tot}}}$ is the equation of state of the Universe. The explicit form of the energy densities and pressures are already given in Eqs. (2.9), (2.10) and (2.11). The Gauss-Bonnet term is written as $R_{\text{GB}}^2 = 24H^2(\dot{H} + H^2) \equiv -24H^4 q$. In particular, it is the scalar field equation (2.16) that makes the continuity equation (2.13) for the sum of the scalar and the Gauss-Bonnet term hold. This can be seen by observing that $\dot{\rho}_{\phi} + 3H(\rho_{\phi} + p_{\phi}) = \dot{\phi}(\ddot{\phi} + 3H\dot{\phi} + V')$ and $\dot{\rho}_{\text{GB}} + 3H(\rho_{\text{GB}} + p_{\text{GB}}) = -24\dot{\phi}f'H^2(\dot{H} + H^2) = -\dot{\phi}f'R_{\text{GB}}^2$.

Then the Friedmann equations take the explicit form:

$$H^2 = \frac{\kappa}{3} \left(\frac{1}{2} \dot{\phi}^2 + V - 24f\dot{H}^3 + \rho_{\text{rad}} \right), \quad (2.19)$$

$$\dot{H} = -\frac{\kappa}{2} \left(\dot{\phi}^2 + 8 \frac{d(f\dot{H}^2)}{dt} - 8f\dot{H}^3 + \rho_{\text{rad}} + p_{\text{rad}} \right), \quad (2.20)$$

$$\ddot{\phi} + 3H\dot{\phi} + V' - 24f'H^2(\dot{H} + H^2) = 0. \quad (2.21)$$

Note that Eq. (2.15) or Eq. (2.20) can be obtained by taking a time derivative of Eq. (2.14) or Eq. (2.19), and using Eq. (2.21) and the continuity equation for radiation.

In Eq. (2.1) the potential $V(\phi)$ is in principle an arbitrary function of ϕ for which a power law or an exponential form is adopted in the literature and that, for instance, plays a crucial role in inflationary scenarios. In our case it represents a non-minimal ingredient that enlarges the number of free parameters without being strictly necessary, while interfering with the peculiar non-linear effect of the GB term on the evolution of the scalar field ϕ that represents the main characteristic of the dEGB scenario that we wish to discuss. Moreover, in order to avoid early accelerated expansion before matter-radiation equivalence it is crucial that V is exactly vanishing or extremely close to zero at $T = T_{\text{BBN}}$, requiring to either tune the scalar field evolution or to adopt an ad-hoc functional form that arbitrarily sets V to zero below some threshold temperature. For these reasons with the goal of naturalness and minimality we choose to assume $V = 0$ in our analysis.

3 WIMP thermal relic density and indirect detection bounds

3.1 WIMP relic density

In the thermal decoupling scenario, the WIMP number density n_χ closely follows its equilibrium value n_{eq} as long as $T/m_\chi \gtrsim 1$, because the rate of WIMP annihilations to SM particles $\Gamma = n_\chi \langle \sigma v \rangle$ is larger than the expansion rate of the Universe H . When $T/m_\chi \lesssim 1$ the equilibrium density n_{eq} becomes exponentially suppressed and eventually, at the freeze-out temperature $T = T_f \simeq m_\chi/20$, the ratio Γ/H drops below 1 and the WIMPs stop annihilating so that their number in a comoving volume remains approximately constant. In the standard scenario, the WIMP freezes out in a radiation background, i.e. when $H \equiv H_{\text{rad}} \sim T^2/M_{PL}$ and the correct prediction for the observed CDM density $\Omega h^2 \simeq 0.12$ is obtained for $\langle \sigma v \rangle_f \simeq 3 \times 10^{-26} \text{ cm}^3 \text{ s}^{-1}$. In particular, for a larger value of $\langle \sigma v \rangle_f$ the WIMPs number density n_χ follows its exponentially suppressed equilibrium value n_{eq} for a longer time, leading to a smaller comoving density at decoupling. This implies that the relic density is anti-correlated to the annihilation rate, i.e. $\Omega h^2 \sim 1/\langle \sigma v \rangle_f$. Expanding $\langle \sigma v \rangle$ in powers of $v^2/c^2 \ll 1$ one gets [55]:

$$\langle \sigma v \rangle \simeq a + 6b \frac{T}{m_\chi}, \quad (3.1)$$

where the contributions from s-wave ($l = 0$) and p-wave ($l = 1$) annihilations are determined by the two constants a and b . In a standard radiation background, WIMPs

completely stop annihilating after freeze-out because the annihilation rate redshifts faster than the Hubble rate. In particular, using $H \sim T^2$ and $n_\chi \sim a^{-3} \sim T^3$ one gets $\Gamma/H_{\text{rad}} = n_\chi \langle \sigma v \rangle / H_{\text{rad}} \sim T$ for s-wave ($a \neq 0$) and $\Gamma/H_{\text{rad}} \sim T^2$ for p-wave ($a = 0$).

A modified cosmological scenario affects the relic density if it changes the Universe expansion rate at the WIMP freeze-out temperature compared to the standard radiation background. In particular, if the WIMP decouples when $H(T') \sim H(T)(T'/T)^\xi$ with $\xi > 2$ the freeze-out condition $\Gamma/H = 1$ is achieved at a larger temperature, so that at fixed $\langle \sigma v \rangle_f$ the relic density is increased. This implies that the correct relic density is achieved for a larger value of $\langle \sigma v \rangle_f$. A more subtle effect [49] is that in this case for $T < T_f$ one has $\Gamma/H \sim T^{3-\xi}$ (s-wave) or $\Gamma/H \sim T^{4-\xi}$ (p-wave) so that if ξ is large enough ($\xi > 3$ for s-wave and $\xi > 4$ for p-wave) the post freeze-out annihilation rate redshifts slower than the Hubble rate. When this happens, at variance with the case when they decouple in a radiation background, the WIMP particles keep annihilating also after freeze-out, substantially reducing the final value of the relic density. This reduction partially mitigates the enhancement effect due to the anticipated freeze-out.

The Boltzmann equation describing the evolution of the WIMP number density is conveniently expressed in terms of the comoving density $Y \equiv n_\chi/s$, with $s = (2\pi^2/45)g_{*s}T^3$ being the entropy density of the Universe and $g_{*s}(T)$ the corresponding number of degrees of freedom, equal to g_* before neutrino decoupling [56]. Indicating with Y_{eq} the corresponding equilibrium value we can write:

$$\frac{dY_\chi}{dx} = -\frac{\beta s}{H x} \langle \sigma v \rangle (Y_\chi^2 - (Y_\chi^{\text{eq}})^2), \quad (3.2)$$

where $x = m_\chi/T$ and:

$$\beta = \left(1 + \frac{1}{3} \frac{d \ln g_s}{d \ln T} \right). \quad (3.3)$$

The temperature evolution of the Hubble parameter is obtained by solving the coupled differential equations for \dot{H} and $\ddot{\phi}$ (Eqs. (2.20) and (2.21), respectively). Assuming isentropic expansion ($sa^3 = \text{constant}$), the change of variable from time to temperature is given as usual as:

$$\frac{dT}{dt} = -\frac{HT}{\beta}. \quad (3.4)$$

In Section 4 we obtain the WIMP comoving density Y_χ^0 at present time in terms of $\langle \sigma v \rangle$ and m_χ by solving Eq. (3.2) numerically. Finally, in terms of Y_χ^0 the WIMP relic density is given by:

$$\Omega_\chi h^2 = \frac{\rho_\chi}{\rho_c} h^2 = 2.755 \times \left(\frac{m_\chi}{\text{GeV}} \right) Y_\chi^0. \quad (3.5)$$

In particular we will indicate with $\langle \sigma v \rangle_{\text{relic}}$ the value of $\langle \sigma v \rangle_f$ that yields the observed value of the present DM relic density, $\Omega_\chi h^2 = 0.12$.

3.2 Indirect detection bounds on WIMP annihilation

The same annihilation processes to SM particles that keep WIMPs in thermal equilibrium in the Early Universe can be used to search for indirect detection signals at later times.

WIMPs annihilations in the halo of our Galaxy can produce various primary SM particles which can further cascade leading to secondary final states such as photons, electrons (positrons), (anti)protons and (anti)neutrinos. Such particles can be looked for using different types of experiments. For example, positrons or antiprotons with energies above a few tens of GeV can be searched for using cosmic-ray spectrometers like AMS [57–59]. On the other hand, gamma-ray telescopes like Fermi LAT [60, 61] can look for gamma rays from WIMP annihilations in the Galactic center or in dwarf spheroidal galaxies (dSphs). Ionizing particles injected by WIMP annihilations can also affect the anisotropies of the Cosmic Microwave Background radiation (CMB) and can be constrained by Planck data [62].

Assuming a self-conjugate WIMP the amount of e^+ or γ -rays with energy E produced by WIMP annihilations per unit time, volume and energy is given by:

$$Q_{e^+/\gamma}(r, E) = \langle\sigma v\rangle_{\text{gal}} \frac{\rho_\chi^2(r)}{2m_\chi^2} \sum_F B_F \frac{dN_{e^+/\gamma}^F}{dE}(E, m_\chi), \quad (3.6)$$

where $\langle\sigma v\rangle_{\text{gal}}$ is the WIMP annihilation cross section in our Galaxy, ρ_χ/m_χ is the number density of DM at the location r of the annihilation process, B_F is the branching fraction to the primary annihilation channel F , while $dN_{e^+/\gamma}^F/dE$ is the e^+/γ energetic spectrum per F annihilation. Depending on m_χ the WIMP primary annihilation channels can be e^+e^- , $\mu^+\mu^-$, $\tau^+\tau^-$, $b\bar{b}$, $t\bar{t}$, $\gamma\gamma$, W^+W^- , ZZ , etc. Gamma rays propagate on a straight line so their signal points back to the source, while the propagation of positrons is bent by the galactic magnetic field and is affected by solar modulation and energy-loss processes along the way [61, 63, 64].

The non-observation of a significant excess over the background allows to use Eq. (3.6) to obtain an upper bound on $\langle\sigma v\rangle_{\text{gal}}$ as a function of m_χ . In particular, in the analysis of Section 4 we will assume the case of s-wave annihilation ($a \neq 0$ in Eq. (3.1)) for which $\langle\sigma v\rangle_{\text{gal}} = \langle\sigma v\rangle_f$, with $\langle\sigma v\rangle_f$ the same annihilation cross section times velocity at freeze-out discussed in Section 3.1.

m_χ [GeV]	$\langle\sigma v\rangle_{\text{ID}}$ [cm^3s^{-1}]
10	1.8×10^{-26}
100	10^{-25}
1000	3×10^{-24}

Table 1. 95% C.L. conservative indirect detection upper-bound $\langle\sigma v\rangle_{\text{ID}}$ on $\langle\sigma v\rangle_{\text{gal}}$ from the analysis of Ref. [64] for the three WIMP mass benchmarks discussed in Section 4.

The bound on $\langle\sigma v\rangle_{\text{gal}}$ depends on the branching fractions B_F , which for a generic WIMP are not fixed. In this case, a conservative bound on $\langle\sigma v\rangle_{\text{gal}}$ has been obtained

in [64] by scanning over all the possible $0 \leq B_F \leq 1$ combinations (with the exception of $F = \text{neutrinos}$) with the constraint $\sum_F B_F = 1$. The authors considered an exhaustive list of existing experiments and took conservative assumptions on the astrophysical backgrounds as well as for various quantities such as the DM density profile, the Galactic magnetic field and diffusion parameter, solar modulation, etc. The resulting 95% C.L. combined limit on $\langle \sigma v \rangle_{\text{gal}}$ is provided in Fig. 5 of [64]. In Table 1 we report from Ref. [64] the numerical values corresponding to the three benchmark WIMP masses $m_\chi = 10 \text{ GeV}$, 100 GeV and 1 TeV that will be used in Section 4 to constrain the allowed parameter space of the dEGB model. In this range of m_χ the bound is mainly determined by the measurement of the positron flux by AMS-02 [57, 58] and that of the gamma-ray flux from dSphs by Fermi LAT [61].

4 Results

4.1 Numerical solutions of Friedmann equations

In this Section, we discuss the numerical solutions of the modified Friedmann equations presented in Section 2. As already pointed out, in our analysis we will assume $V(\phi) = 0$ and the dEGB function $f(\phi)$ defined in Eq. (2.2). As a consequence, the WIMP decoupling mechanism is expected to be modified compared to the standard case. In particular, introducing the enhancement parameter:

$$A(T) \equiv \frac{H(T)}{H_{\text{rad}}}, \quad (4.1)$$

if $\rho_{\text{tot}} > \rho_{\text{rad}}$ through Eq. (2.19) one has $A > 1$ and the $\langle \sigma v \rangle_f = \langle \sigma v \rangle_{\text{relic}}$ corresponding to the observed relic density is driven to higher values compared to the standard case. This will be used in Section 4.2.2 to constrain the dEGB parameter space using the bounds from WIMP indirect searches. The results of this Section rely on numerical solutions. In Appendix A a qualitative insight on such solutions is provided making use of some semi-analytical approximations.

We rewrite the Friedmann equations in Eqs. (2.19), (2.20) and (2.21) for reference:

$$H^2 = \frac{\kappa}{3} \left(-24f'\dot{\phi}H^3 + \frac{1}{2}\dot{\phi}^2 + \rho_{\text{rad}} \right), \quad (4.2)$$

$$\dot{H} = -\frac{\kappa}{2} \left(\dot{\phi}^2 + 8\frac{d(f'\dot{\phi}H^2)}{dt} - 8f'\dot{\phi}H^3 + \rho_{\text{rad}} + p_{\text{rad}} \right), \quad (4.3)$$

$$\ddot{\phi} + 3H\dot{\phi} + V'_{\text{GB}} = 0, \quad (4.4)$$

where:

$$V'_{\text{GB}} \equiv -f'R_{\text{GB}}^2 = -24f'H^2(\dot{H} + H^2) = 24\alpha\gamma e^{\gamma\phi} qH^4, \quad (4.5)$$

is technically not the gradient of a potential, but just an excess of notation to indicate that it drives the scalar field evolution, while $q = (1 + 3w)/2$ is the usual deceleration parameter in (2.18) ($q = 1$ for radiation dominance at T_{BBN}). We present our results in

geometric units (defined as $\kappa = 8\pi G = 1$, $c = 1$) in which α is in m^2 and ϕ as well as γ are dimensionless.

Equations (4.3) and (4.4) can be re-arranged into a set of three first order coupled differential equations for the quantities ϕ , $\dot{\phi}$ and H . We set the boundary conditions on $\phi(T_{\text{BBN}}) \equiv \phi_{\text{BBN}}$, $\dot{\phi}(T_{\text{BBN}}) \equiv \dot{\phi}_{\text{BBN}}$ and $H(T_{\text{BBN}}) \equiv H_{\text{BBN}}$ at the BBN temperature, assumed to be $T = T_{\text{BBN}} = 1$ MeV. Note that a shift of ϕ_{BBN} is equivalent to a redefinition of the α parameter thanks to the fact that $V(\phi) = 0$ and the scalar field ϕ (and hence ϕ_{BBN}) appears in the Friedmann equations (4.2)-(4.4) only through $f(\phi)$:

$$\phi'_{\text{BBN}} = \phi_{\text{BBN}} + \phi_0, \quad \alpha' = \alpha e^{-\gamma\phi_0}, \quad \gamma' = \gamma. \quad (4.6)$$

In other words, any choice of ϕ_{BBN} corresponds to a specific gauge fixing and the quantity:

$$\tilde{\alpha} = \alpha e^{\gamma\phi_{\text{BBN}}}, \quad (4.7)$$

is invariant under the gauge transformation (4.6). In our analysis, we will show our results in terms of $\tilde{\alpha}$ (which is equivalent to adopt the gauge $\phi_{\text{BBN}} = 0$). Notice that the boundary condition on $H(T_{\text{BBN}}) = H_{\text{BBN}}$ can be obtained from $\phi_{\text{BBN}} (= 0)$ and $\dot{\phi}_{\text{BBN}}$ by solving the cubic equation Eq. (4.2) at T_{BBN} :

$$\begin{aligned} AH_{\text{BBN}}^3 + H_{\text{BBN}}^2 - B &= 0, \\ A &= 8\kappa f'(\phi_{\text{BBN}})\dot{\phi}_{\text{BBN}}, \\ B &= \frac{\kappa}{3} \left[\frac{1}{2}\dot{\phi}_{\text{BBN}}^2 + \rho_{\text{rad}}(T_{\text{BBN}}) \right], \end{aligned} \quad (4.8)$$

and taking the positive solution closer to $H_{\text{rad}}(T_{\text{BBN}})^2$. The only boundary condition taking arbitrary value is then $\dot{\phi}_{\text{BBN}}$, which can be chosen to be positive (or zero). This is because the configurations with $\dot{\phi}_{\text{BBN}} < 0$ are obtained when $\gamma \rightarrow -\gamma$ since the solutions of the Friedmann equations become invariant under a simultaneous change of sign of $\dot{\phi}_{\text{BBN}}$ and γ .

The contribution of $\rho_\phi(T_{\text{BBN}}) = \frac{1}{2}\dot{\phi}_{\text{BBN}}^2$ to the energy density at BBN is constrained by the upper bound on the effective number of neutrino flavors $N_{\text{eff}} \leq 2.99 \pm 0.17$ [65], that can be converted into $\rho_\phi(T_{\text{BBN}}) \leq 3 \times 10^{-2}\rho_{\text{BBN}}$, with ρ_{BBN} the standard radiation energy density at BBN. In Section 4.2.2, we will adopt three nonnegative benchmarks for $\dot{\phi}_{\text{BBN}}$ corresponding to $\rho_\phi(T_{\text{BBN}}) = 0$, the upper bound $\rho_\phi(T_{\text{BBN}}) = 3 \times 10^{-2}\rho_{\text{BBN}}$ and an illustrative intermediate value $\rho_\phi(T_{\text{BBN}}) = 10^{-4}\rho_{\text{BBN}}$.

Once the boundary condition for $\dot{\phi}_{\text{BBN}}$ is given for one of the three benchmarks above with the gauge $\phi_{\text{BBN}} = 0$ and H_{BBN} from Eq. (4.8), the solutions of the set of the three first order coupled differential equations for ϕ , $\dot{\phi}$ and H are obtained for given values of the parameters $\tilde{\alpha}$ and γ by evolving them numerically from $T_{\text{BBN}} = 1$ MeV to higher temperatures (we stop at $T = 100$ TeV). The temperature evolution can be obtained by changing variable from t to T using Eq. (3.4).

²Notice that a cubic equation as always at least one real solution. We find more convenient to include the expression of \dot{H} to the set of differential equations. An alternative way to obtain the evolution of $H(T)$ is to solve the cubic equation (4.2), which is valid at all temperatures, in terms of $\phi(T)$ and $\dot{\phi}(T)$.

In the remaining part of this Section we illustrate numerical solutions and show with some examples how Cosmology is modified at $T > T_{\text{BBN}}$ by the dEGB scenario.

In Figs. 1 and 2 we show the evolution of the energy density of the Universe ρ_{tot} and of its different contributions, as indicated in Eq. (4.2), for the benchmark values $\tilde{\alpha} = \pm 1 \text{ km}^2$, $\gamma = \pm 1$. Note that only ρ_{tot} and ρ_{rad} represent physical energy densities, while ρ_{ϕ} and ρ_{GB} are shown for illustrative purposes (in particular, ρ_{GB} can be negative and is plotted in absolute value).

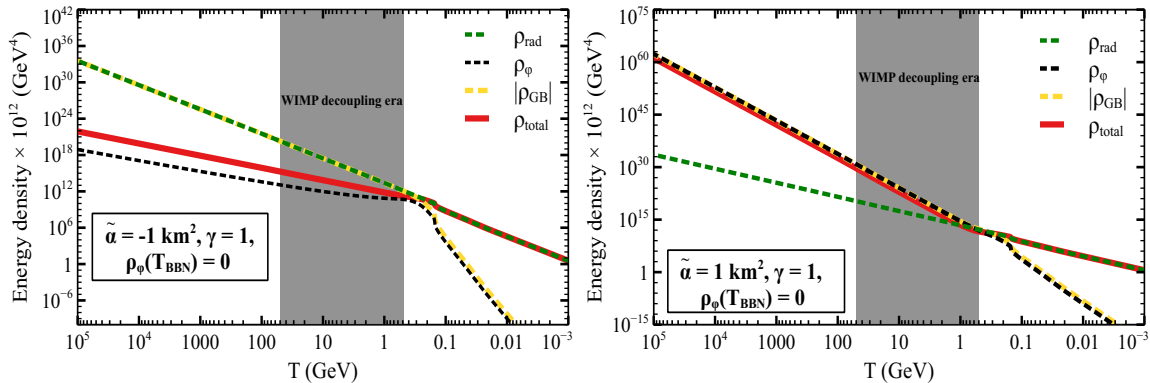


Figure 1. Evolution of ρ_{rad} , ρ_{ϕ} , ρ_{GB} and ρ_{total} with T for $\rho_{\phi}(T_{\text{BBN}}) = 0$ and $\phi(T_{\text{BBN}}) = 0$.

In Figs. 3 and 4 the equation of state of the Universe $w_{\text{tot}} = p_{\text{tot}}/\rho_{\text{tot}}$ as well as those of the separate components $w_i = p_i/\rho_i$ are shown for the same benchmark values of $\tilde{\alpha}$ and γ , with $\rho_{\phi}(T_{\text{BBN}}) = 0$ and $\rho_{\phi}(T_{\text{BBN}}) = 3 \times 10^{-2} \rho_{\text{BBN}}$, respectively. Notice that in some cases $w_{\{\phi+GB\}}$ diverges because $\rho_{\{\phi+GB\}}$ changes sign. However $\rho_{\{\phi+GB\}}$ maintains a smooth temperature behaviour. In particular the relation $\rho_i \propto T^{3(1+w_i)}$ only holds when w_i is constant and for components that verify separately the continuity equation. In Figs. 1 and 3, where $\rho_{\phi}(T_{\text{BBN}}) = 0$, plots for only $\gamma = 1$ are provided since those for $\gamma = -1$ are identical. Moreover, two examples of the values reached by the enhancement parameter of Eq. (4.1) at the temperature $T = 50 \text{ GeV}$ are provided in Fig. 6 in the $\tilde{\alpha}$ - γ plane, for $\rho_{\phi}(T_{\text{BBN}}) = 0$ (left-hand plot) and $\rho_{\phi}(T_{\text{BBN}}) = 3 \times 10^{-2}$ (right-hand plot). Notice that, as explained in the case of Figs. 1 and 3, the left hand plot in Fig. 6 is symmetric under a change of sign of the γ parameter.

The region shaded in gray between the two vertical solid lines in Figs. 1 to 4 represents the interval of temperatures where the WIMP decoupling takes place ($500 \text{ MeV} < T < 50 \text{ GeV}$ for the WIMP mass interval $10 \text{ GeV} < m_{\chi} < 1 \text{ TeV}$ and $T_f \sim m_{\chi}/20$). In all the plots for this range of temperatures, ρ_{tot} (the solid red line) differs from ρ_{rad} (the dotted green line) that represents the evolution of the energy density in the case of radiation domination i.e., Standard Cosmology.

As a reference, let us consider the solution for $\tilde{\alpha}$ and/or $\gamma = 0$ (i.e., for a theory of the radiation and the scalar kinetic term with vanishing dEGB term). The radiation density evolves as $\rho_{\text{rad}} \sim T^4$ over the whole temperature range. On the other hand, the generally complicated (photon) temperature dependence of the scalar field kinetic energy (kination)

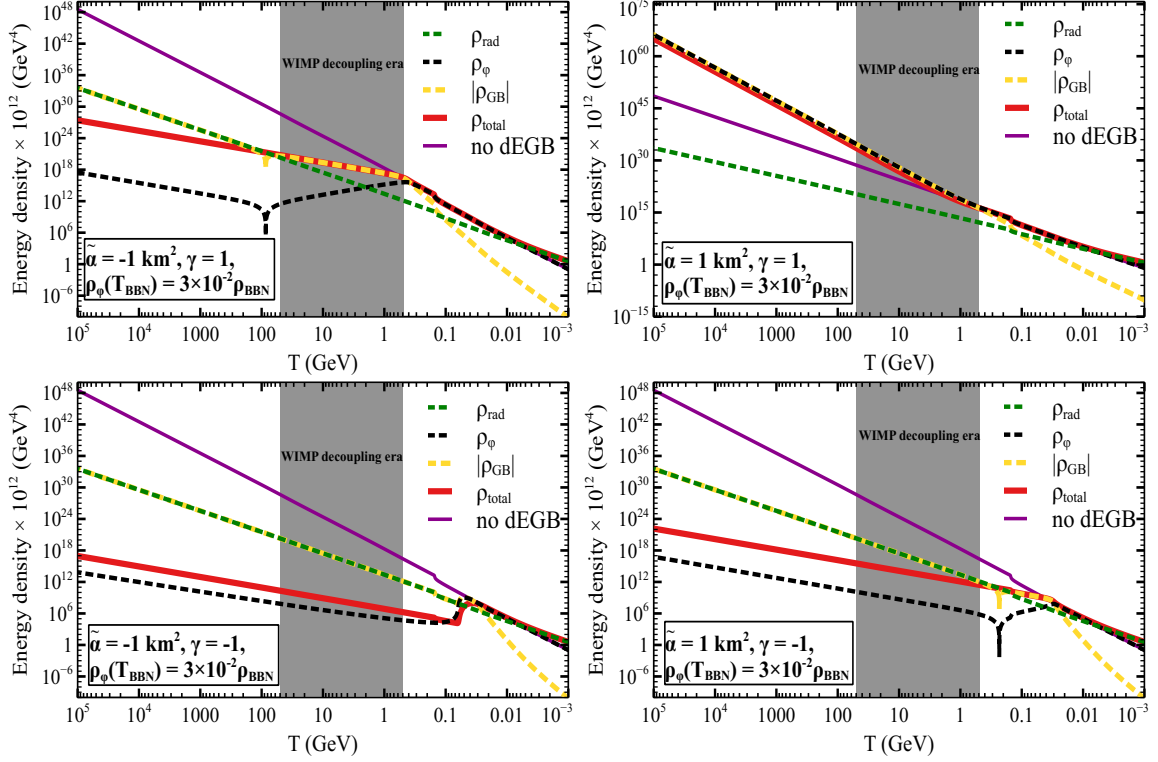


Figure 2. Evolution of ρ_{rad} , ρ_{ϕ} , ρ_{GB} and ρ_{total} with T for $\rho_{\phi}(T_{\text{BBN}}) = 3 \times 10^{-2} \rho_{\text{BBN}}$ and $\phi(T_{\text{BBN}}) = 0$. Recall that only ρ_{rad} and ρ_{total} are physical quantities.

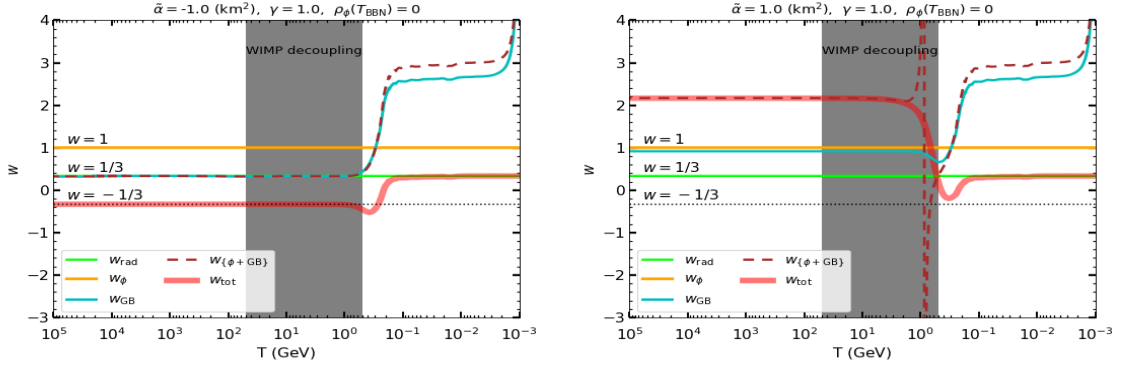


Figure 3. Temperature evolution of the equation of state $w (= p/\rho)$ for the Universe and for different components.

can be shown to be simplified as $\rho_{\phi} \sim T^6$ in the region where either the radiation or the scalar field (kination) dominates. This is shown in purple in Fig. 2 (this case corresponds to radiation dominance in Fig. 1). As a consequence, for $\rho_{\phi}(T_{\text{BBN}}) \lesssim \epsilon \rho_{\text{BBN}}$ the energy density of kination drives the Universe expansion for $T \gtrsim T_{\text{cross}} = T_{\text{BBN}}/\sqrt{\epsilon}$, with the enhancement factor $A(T) = \sqrt{1 + \epsilon(T/T_{\text{BBN}})^2}$. For $\epsilon = 3 \times 10^{-2}$ one gets $T_{\text{cross}} \simeq 5.8 \text{ MeV}$

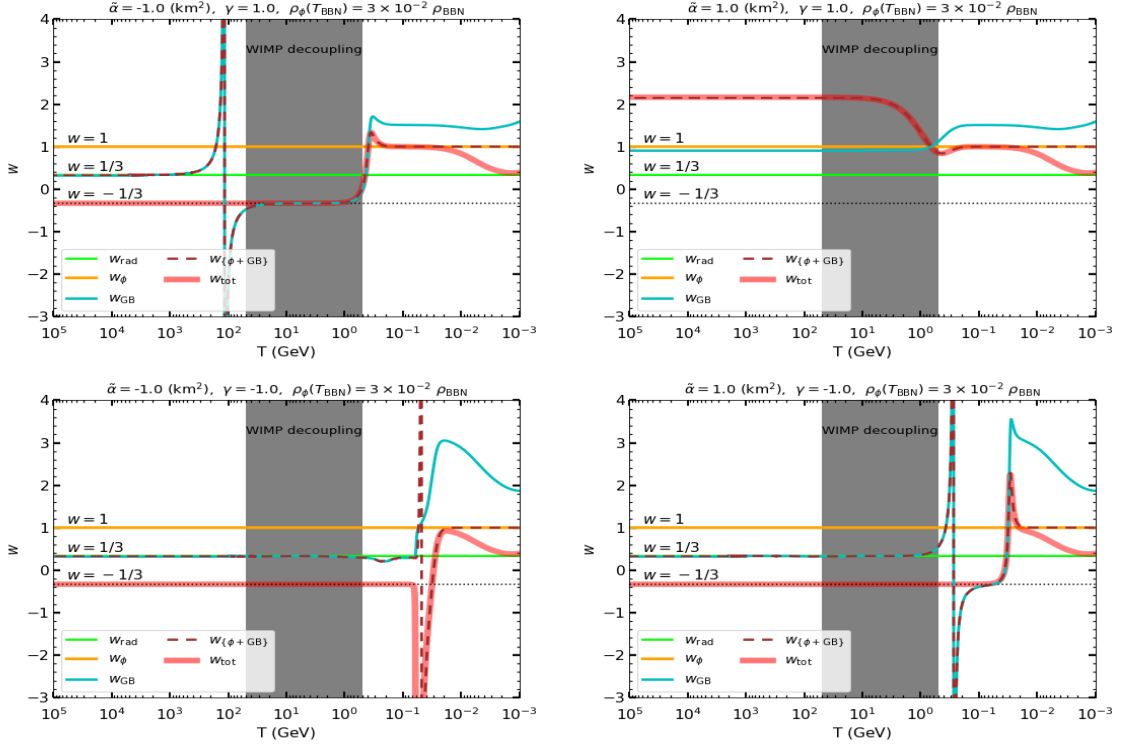


Figure 4. The same as in Fig. 3 for $\rho_\phi(T_{\text{BBN}}) = 3 \times 10^{-2} \rho_{\text{BBN}}$.

and $80 \lesssim A(T) \lesssim 8000$ in the temperature range of WIMP decoupling, $500 \text{ MeV} \leq T \leq 50 \text{ GeV}$. To predict the correct relic abundance such high enhancement factors require values of $\langle \sigma v \rangle_{\text{gal}} = \langle \sigma v \rangle_{\text{f}}$ that exceed the bound discussed in Section 3.2 unless $\rho_\phi(T_{\text{BBN}})$ is much smaller than its upper bounds from BBN. This is shown in Fig. 5, where, for a vanishing dEGB term (kination only), the upper bound on $\rho_\phi(T_{\text{BBN}})$ from WIMP indirect detection is plotted as a function of m_χ and compared to the two representative non-vanishing values that will be used in the quantitative analysis of Section 4.2.2, $\rho_\phi(T_{\text{BBN}}) = 3 \times 10^{-2} \rho_{\text{BBN}}$ and $\rho_\phi(T_{\text{BBN}}) = 10^{-4} \rho_{\text{BBN}}$. Fig. 5 shows that in absence of the dEGB term both values are excluded. On the other hand, in Section 4.2.2 we will show that many combinations of $\tilde{\alpha} \neq 0$, $\gamma \neq 0$ are allowed for the same two values of $\rho_\phi(T_{\text{BBN}})$. This clearly indicates that for such configurations the dEGB term plays a mitigating role on the kination dynamics, slowing down the speed of the scalar field evolution and reducing in this way the predicted values of the enhancement factor $A(T)$. Notice also that for $\tilde{\alpha}$ and/or $\gamma = 0$ (kination only) ρ_ϕ vanishes at all temperatures if $\rho_\phi(T_{\text{BBN}}) = 0$, while this is no longer true in presence of the dEGB term.

Note that T_{cross} becomes higher as ϵ becomes smaller. Actually, when $\epsilon = 0$, i.e., kination at T_{BBN} is zero, $\dot{\phi}(T)$ becomes identically zero, reducing to Standard Cosmology where the evolution of the Universe is simply given by radiation. Hence, the enhancement factor $A(T) \equiv 1$. This can be seen on the axes of the left hand plot of Fig. 6, where $\tilde{\alpha}\gamma = 0$.

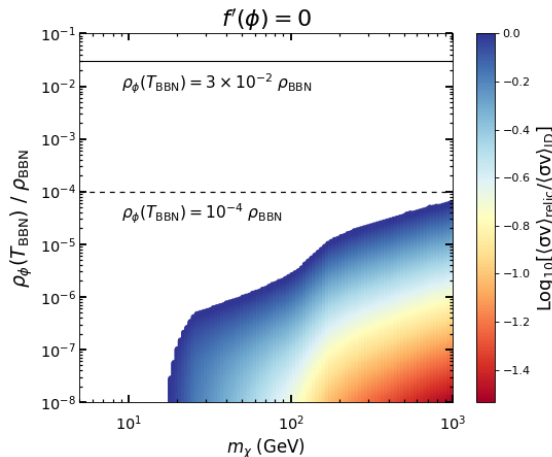


Figure 5. Values of $\rho_\phi(T_{\text{BBN}})$ favoured by WIMP indirect detection (ID) searches are shown by color coding for m_χ in the range 5 GeV - 1 TeV. Here both $f'(\phi)$ and $V(\phi)$ are kept at zero. The three benchmark values of $\rho_\phi(T_{\text{BBN}})$ used in this work are $\rho_\phi(T_{\text{BBN}}) = 0$, $10^{-4} \rho_{\text{BBN}}$ (shown by the black dashed line) and $3 \times 10^{-2} \rho_{\text{BBN}}$ (the black solid line). The color code of the shaded areas is the same as in Figs. 7 and 8 and explained in Section 4.2.2.

We now investigate the numerical solutions plotted in Figs. 1 and 2. Near $T = T_{\text{BBN}}$ the dEGB term is negligible and radiation dominates. The Hubble parameter grows as $H \sim T^2$, while $\dot{\phi} \sim T^3$ and $\rho_\phi \sim T^6$, which grows faster than $\rho_{\text{rad}} \sim T^4$. So radiation domination is followed by an era dominated by kination at $T \gtrsim T_{\text{cross}} \sim 5.8$ MeV. This qualitative analysis shows consistency with Figs. 1 and 2. However, at higher temperatures the presence of the dEGB term has peculiar non-linear effects on the evolution of ϕ and $\dot{\phi}$ that significantly modify the energy density of the Universe and of the enhancement factor $A(T)$ compared to the scenario of simple kination. In particular ρ_{GB} quickly becomes of the same order of ρ_ϕ , since at this stage its equation of state is much larger than any other component (see Fig. 4 and Appendix A.1). In order to understand what happens at higher temperatures we analyse Eq. (4.4): in particular the largest values for the enhancement parameter are reached when $\dot{\phi}$ grows faster with T than kination in the interval of temperatures relevant for the WIMP decoupling.

The case $\dot{\phi}_{\text{BBN}} = 0$ is shown in Fig. 1. The invariance by the transformation $\dot{\phi}_{\text{BBN}} \rightarrow -\dot{\phi}_{\text{BBN}}$, $\gamma \rightarrow -\gamma$ implies that the results do not depend on the sign on γ (except that $\dot{\phi} \rightarrow -\dot{\phi}$), so only $\gamma = 1$ is shown, for both signs of $\tilde{\alpha}$. For $\tilde{\alpha} > 0$ (right-hand plot) at T_{BBN} one has $V'_{\text{GB}} > 0$ in the scalar field equation of motion, so that $\ddot{\phi} < 0$ and $d\dot{\phi}/dT > 0$. This means that $\dot{\phi}$ grows positive with T (so that $3H\dot{\phi} \geq 0$ and $\rho_{\text{GB}} < 0$) which implies that $d\phi/dT < 0$ and that ϕ grows negative, with kination domination close to T_{BBN} with $3H\dot{\phi} \gg V'_{\text{GB}}$. As ϕ grows negative with T both ρ_{GB} and V'_{GB} get suppressed by the exponential term $e^{\gamma\phi}$, so that V'_{GB} does not affect the field evolution and ρ_{GB} is never competing with ρ_ϕ to drive the Universe expansion. As a consequence, at high temperature the energy of the Universe is driven by kination and as shown in the left-hand plot of Fig. 6 the enhancement factor at high temperature is higher than unity.

On the other hand, for $\tilde{\alpha} < 0$ the left-hand plot of Fig. 1 shows that ρ_ϕ stops growing and indeed in the left-hand plot of Fig. 6 the enhancement factor turns out to be below unity. This may appear surprising, since at T_{BBN} both $3H\dot{\phi}$ and V'_{GB} are negative, with V'_{GB} enhanced by the $e^{\gamma\phi}$ term, so nothing apparently prevents a large growth of $\dot{\phi}$ with kination domination and large A values. In particular, one now has $V'_{\text{GB}} < 0$, so $\ddot{\phi} > 0$ and $d\dot{\phi}/dT < 0$ which implies that $\dot{\phi}$ develops a negative value and also $3H\dot{\phi} < 0$, with $\rho_{\text{GB}} < 0$, $d\rho/dT > 0$ and $\phi > 0$. So again, as in the previous case, $3H\dot{\phi}$ and V'_{GB} have the same sign and initially kination dominates. However, at variance with the case with $\tilde{\alpha} > 0$, now ρ_{GB} is negative and exponentially enhanced, grows much faster than ρ_ϕ and reaches it very quickly. When this happens $\rho_{\{\phi+\text{GB}\}}$ must remain positive, so a large cancellation between ρ_{GB} and ρ_ϕ is achieved, which is sufficient to flatten the temperature dependence of $\rho_{\text{tot}} \simeq \rho_{\{\phi+\text{GB}\}}$ and trigger an era of accelerated expansion (indeed, in Fig. 3 the equation of state of the Universe drops below $-1/3$). This changes the sign of the deceleration parameter q and so of V'_{GB} that depends on it (see Eq. (4.4)), so that $\dot{\phi}$ starts decreasing, kination dominance stops and $A < 1$. This back-reaction mechanism is discussed in more detail in Appendix A.2 with the help of a semi-analytical approximation. Such results, obtained for the specific case $\tilde{\alpha} = \pm 1 \text{ km}^2$ and $\gamma = \pm 1$ are confirmed for a wider range of the parameters. In particular the highest sensitivity is on γ , that enters in the exponent of $f(\phi)$. For $\tilde{\alpha} > 0$ $f(\phi)$ is exponentially suppressed, so increasing γ leads to a further suppression with no effect on the evolution of ϕ . On the other hand, for $\tilde{\alpha} < 0$ the function $f(\phi)$ is exponentially enhanced, so increasing γ accelerates the back-reaction effect, that shifts to lower temperatures, again with little effect on the evolution of ϕ at high temperatures. This is confirmed by the left-hand plot of Fig. 6, that provides for $\dot{\phi}_{\text{BBN}} = 0$ a scan of the enhancement factor at $T = 50 \text{ GeV}$ in the $\tilde{\alpha}$ - γ plane (note that in this plot the region close to the axes, $\tilde{\alpha}\gamma \rightarrow 0$, corresponds to Standard Cosmology, i.e. $A = 1$). Indeed, from this plot one can qualitatively conclude that, at least at large-enough temperatures, $A(T) > 1$ for $\tilde{\alpha} > 0$ and $A(T) < 1$ for $\tilde{\alpha} < 0$.

The situation for $\rho_\phi(T_{\text{BBN}}) \neq 0$ is shown in Fig. 2, where the value $\rho_\phi(T_{\text{BBN}}) = 3 \times 10^{-2} \rho_{\text{BBN}}$ is shown. Since $\dot{\phi}_{\text{BBN}} > 0$ in all the four possible cases ϕ grows negative with T for $T \gtrsim T_{\text{BBN}}$, the exponential $e^{\gamma\phi}$ is suppressed for $\gamma > 0$ (upper plots) and enhanced for $\gamma < 0$ (lower plots). Near $T \gtrsim T_{\text{BBN}}$ the Gauss-Bonnet effect is small and $3H\dot{\phi} > 0$ and so $\ddot{\phi}_{\text{BBN}} < 0$ in all the four possible cases. For $\tilde{\alpha}, \gamma > 0$ (upper-right) and $V'_{\text{GB}} > 0$ (same sign of $3H\dot{\phi}$), $\ddot{\phi}$ never changes sign and kination dominates at high temperature since ρ_ϕ never stops growing. This case corresponds to the situation with the highest enhancement factor. This is reflected in the right-hand plot of Fig. 6, where the value of the enhancement factor at $T = 50 \text{ GeV}$ ranges between 10^4 and 10^8 for both $\tilde{\alpha}$ and γ positive. On the other hand, for all the other three sign combinations of $\tilde{\alpha}$ and γ kination stops dominating the Universe expansion at some stage, implying at the corresponding temperatures enhancement factors either moderate or less than unity. The two cases when $\tilde{\alpha}\gamma < 0$ are easier to understand: now $V'_{\text{GB}} < 0$, so eventually $\ddot{\phi}$ changes sign and $\dot{\phi}$ starts decreasing. This suppresses ρ_ϕ (that is quadratic in $\dot{\phi}$) more than ρ_{GB} (which is linear) so that kination dominance stops and a short era driven by ρ_{GB} (that at this stage is positive) starts, for which $A(T) > 1$. However, this condition does not last much since at higher temperature $\dot{\phi}$ keeps decreasing

and eventually crosses zero, so that both ρ_ϕ and ρ_{GB} vanish, leading the way to a short period of radiation domination, eventually followed by one driven by $\rho_{\text{rad}} + \rho_{\text{GB}} < \rho_{\text{rad}}$ (with $A < 1$), when $\dot{\phi}$ and ρ_{GB} get negative and large enough in absolute value.

At even larger T the sign flip in $\dot{\phi}$ implies that the scalar field ϕ eventually becomes positive. What happens at this stage depends on the sign of γ . In particular, for $\gamma > 0$ the dominance of $\rho_{\text{rad}} + \rho_{\text{GB}}$ continues, because the exponential term in ρ_{GB} and V'_{GB} remains large. However, for $\gamma < 0$ the V'_{GB} term is exponentially suppressed and the evolution of $\dot{\phi}$ is again only driven by $3H\dot{\phi}$, triggering another period dominated by kination with $A > 1$. Indeed, in the two panels with $\tilde{\alpha}\gamma < 0$ the enhancement factor $A(T)$ is in general small or moderate, corresponding to the phase when the expansion of the Universe is driven by $\rho_{\text{rad}} + \rho_{\text{GB}} < \rho_{\text{rad}}$. However, for $\gamma < 0$ larger values of $|\gamma|$ drive A above unity. This happens because for $\gamma > 0$ a larger γ slows down the scalar field evolution delaying the epoch dominated by ρ_{GB} to a higher range of temperatures that includes $T = 50$ GeV. On the other hand, when $\gamma < 0$ and large enough in absolute value the scalar field evolution is faster, anticipating to $T = 50$ GeV the second epoch of kination dominance triggered at high temperatures when ϕ becomes positive.

The final case that remains to be discussed is that with both $\tilde{\alpha}$ and γ negative, which corresponds to the bottom-left plot of Fig. 2. As confirmed by the right-hand plot of Fig. 6, in this case the evolution of the enhancement factor turns out to be below unity. This case is similar to the left-hand plot of Fig. 1 with $\rho_\phi(T_{\text{BBN}}) = 0$ and $\tilde{\alpha} < 0$. In fact also in this case at T_{BBN} the two quantities V'_{GB} and $3H\dot{\phi}$ have the same sign, with $\rho_{\text{GB}} < 0$ and both GB terms exponentially enhanced. As a consequence, just above T_{BBN} an epoch of kination domination starts, but very quickly $\rho_{\text{GB}} < 0$ reaches the level of ρ_ϕ and the Universe expansion is driven by $\rho_{\text{tot}} = \rho_{\{\phi+\text{GB}\}}$, with a level of cancellation between ρ_{GB} and ρ_ϕ sufficient to flatten the temperature dependence of ρ_{tot} and trigger an era of accelerated expansion (indeed, in Fig. 4 the equation of state of the Universe drops below $-1/3$).

4.2 Constraints on the dEGB scenario

In this Section we will discuss the bounds on the dEGB scenario that can be obtained from the GW signals produced in compact binary mergers and those from WIMP indirect detection that are the main topic of our analysis.

Other classes of bounds that are usually applied on extensions of GR but that do not impose competitive constraints on the dEGB scenario include tests of gravity within the Solar System [66], deviations of Kepler's formula for the motion of binary-pulsar systems [67] and constraints on dipole radiation emission from binary pulsars [67].

4.2.1 Black hole and neutron star binaries

The existence of black hole solutions in the 4D effective superstring action in presence of Gauss-Bonnet quadratic curvature terms [17] has triggered the study of the constraints that can be obtained on dEGB gravity from the observation of Gravitational Waves from BH-BH and BH-NS merger events. In particular, the waveforms obtained by modelling the different phases of compact binaries (inspiral [68], merger [69] and ringdown [70]) in

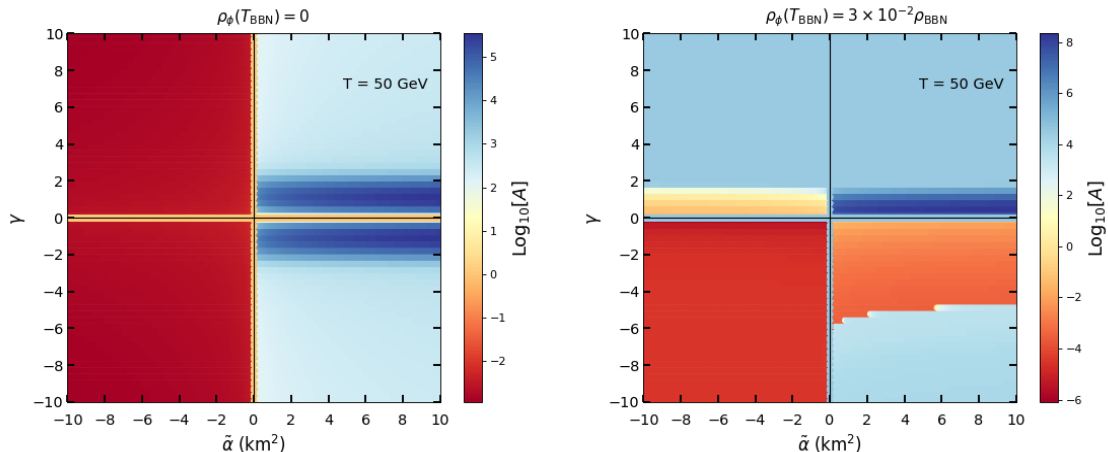


Figure 6. Regions in the Gauss-Bonnet parameter space (spanned by $\tilde{\alpha}$ and γ) that correspond to different values of the enhancement factor A ($= H/H_{\text{rad}}$) at $T = 50$ GeV are shown by different colors. The color bars indicate the values of $\text{Log}_{10}[A]$. *Left column:* $\rho_\phi(T_{\text{BBN}}) = 0$; *Right column:* $\rho_\phi(T_{\text{BBN}}) = 3 \times 10^{-2} \rho_{\text{BBN}}$. Note that here we choose only the positive value of $\dot{\phi}_{\text{BBN}}$ in $\rho_\phi(T_{\text{BBN}})$. The corresponding results for the same but negative value of $\dot{\phi}$ can be obtained from these ones by flipping the sign of γ .

the presence of dEGB gravity can be compared to the data and constraints consistent with the statistical noise on the size of the dEGB deviation from standard GR can be obtained.

Following this procedure, it is already possible to use the data from the LIGO-Virgo Collaboration [71] to put constraints on deviations from GR. For a list of the events from which this has been carried out please check [34–38]. From these studies it is possible to obtain a constraint on the GB term, α_{GB} in the notation of [38], of the order of $\alpha_{\text{GB}}^{1/2} \leq \mathcal{O}(2 \text{ km})$. In particular, for our analysis we use the value $\alpha_{\text{GB}}^{1/2} \leq 1.18 \text{ km}$ [38].

Due to the Universe expansion even if $\dot{\phi}(T_{\text{BBN}}) \neq 0$ the evolution of the scalar field ϕ eventually freezes at some asymptotic temperature $T_L \ll T_{\text{BBN}}$ to a constant background value $\phi(T_L)$, implying no departure from GR at the cosmological level for $T < T_L$. On the other hand, in the vicinity of a BH or a NS the density profile of the scalar field is distorted compared to $\phi(T_L)$, leading to a local departure from GR that can modify the GW signal if the stellar object is involved in a merger event. Near the black hole or the neutron star the distortion of the scalar field is small and the dEGB function $f(\phi)$ can be expanded up to the linear term in the small perturbation $\Delta\phi$ around the asymptotic value $\phi(T_L)$ of the scalar field at large distance [38]:

$$f(\phi) = f(\phi(T_L)) + f'(\phi(T_L)) \Delta\phi + \mathcal{O}((\Delta\phi)^2). \quad (4.9)$$

In this way the constraints from compact binary mergers is expressed in terms of $f'(\phi(T_L))$:

$$|f'(\phi(T_L))| \leq \sqrt{8\pi} \alpha_{\text{GB}}^{\text{max}}, \quad (4.10)$$

with $\alpha_{\text{GB}}^{\text{max}} = (1.18)^2 \text{ km}^2$ [38]. Note that the extra factor of $\sqrt{8\pi}$ in the equation above is due to the conversion from the units of Ref. [38] (that use $G = c = 1$) to those of the present work (where $\kappa = 8\pi G = c = 1$).

At $T \lesssim T_{\text{BBN}}$ V'_{GB} is completely negligible and the scalar field equation is homogeneous, $\ddot{\phi} + 3H\dot{\phi} = a^3 d/dt(a^3\dot{\phi}) = 0$. This implies that if $\dot{\phi}(T_{\text{BBN}}) = 0$ one has $\dot{\phi} = 0$ also below T_{BBN} and as a consequence Eq.(4.10) can be directly used with $\phi(T_L) = \phi(T_{\text{BBN}})$ to put constraints on the $\tilde{\alpha}$ and γ parameters. The regions of the $\tilde{\alpha}$ - γ parameter space that are disallowed by the ensuing constraint correspond to the hatched areas in the left-hand plots of Fig. 7.

However, if $\dot{\phi}(T_{\text{BBN}}) \neq 0$ one needs to consider the residual evolution of ϕ below T_{BBN} to calculate the value of the field $\phi(T_L)$ to be used in Eq. (4.10). In order to do so the derivative of ϕ with respect to the temperature can be expressed as:

$$\frac{d\phi}{dT} = \dot{\phi} \frac{dt}{dT} \simeq -\frac{\dot{\phi}}{HT}, \quad (4.11)$$

where in the last equality Eq. (3.4) with $\beta \sim 1$ has been used. Then neglecting V'_{GB} the evolutions of $\dot{\phi}$ and H below T_{BBN} are simply:

$$\dot{\phi}(T) \simeq \dot{\phi}_{\text{BBN}} \left(\frac{T}{T_{\text{BBN}}} \right)^3, \quad (4.12)$$

$$H(T) \simeq H_{\text{BBN}} \left(\frac{T}{T_{\text{BBN}}} \right)^2, \quad (4.13)$$

assuming that the Universe expansion is driven by radiation at T_L . Plugging the two expressions above in Eq. (4.11) one gets:

$$\frac{d\phi}{dT} = -\frac{\dot{\phi}_{\text{BBN}}}{H_{\text{BBN}}T_{\text{BBN}}}, \quad (4.14)$$

which upon integration from T_{BBN} to T_L yields:

$$\begin{aligned} \phi(T_L) - \phi(T_{\text{BBN}}) &= -\frac{\dot{\phi}_{\text{BBN}}}{H_{\text{BBN}}T_{\text{BBN}}}(T_L - T_{\text{BBN}}) \\ &= \frac{\dot{\phi}_{\text{BBN}}}{H_{\text{BBN}}T_{\text{BBN}}}(T_{\text{BBN}} - T_L) \\ &\simeq \frac{\dot{\phi}_{\text{BBN}}}{H_{\text{BBN}}} \quad [\text{for } T_L \ll T_{\text{BBN}}]. \end{aligned} \quad (4.15)$$

So the value of $\phi(T_L)$ that must be used in Eq. (4.10) is, finally:

$$\phi(T_L) \simeq \phi_{\text{BBN}} + \frac{\dot{\phi}_{\text{BBN}}}{H_{\text{BBN}}}. \quad (4.16)$$

Using this Eq. (4.10) becomes:

$$|\tilde{\alpha}\gamma e^{\gamma \frac{\dot{\phi}_{\text{BBN}}}{H_{\text{BBN}}}}| \leq \sqrt{8\pi} \alpha_{\text{GB}}^{\text{max}}, \quad (4.17)$$

with $\tilde{\alpha}$ defined in Eq. (4.7).

The expression above is used to determine the hatched excluded regions in the right-hand plot of Fig. 7 and in Fig. 8 for $\rho_\phi(T_{\text{BBN}}) = 3 \times 10^{-2} \rho_{\text{BBN}}$ and for $\rho_\phi(T_{\text{BBN}}) = 10^{-4} \rho_{\text{BBN}}$, respectively.

4.2.2 WIMP indirect detection

In this Section we identify the regions of the Gauss-Bonnet parameter space that are favoured or disfavoured by WIMP dark matter. The favoured parameter regions are those for which the predicted WIMP relic density falls within the observational range, $\Omega_\chi h^2 \simeq 0.12$, while at the same time the WIMP annihilation cross section in the halo of our Galaxy is compatible with indirect signals. In particular, for a given choice of the parameters we find the value $\langle\sigma v\rangle_{\text{relic}}$ of $\langle\sigma v\rangle_f$ which yields $\Omega_\chi h^2 \simeq 0.12$ and compare it with the upper bound on the present annihilation cross section in the Milky Way $\langle\sigma v\rangle_{\text{ID}}$ from DM indirect detection searches (see Table 1 and the discussion in Section 3.2). In order to do so we consider an s -wave annihilation cross section, for which $\langle\sigma v\rangle_{\text{gal}} = \langle\sigma v\rangle_f$.

In Figs. 7 and 8 the different colors in the $\tilde{\alpha}$ - γ plane correspond to values of logarithmic ratio, $\text{Log}_{10}[\langle\sigma v\rangle_{\text{relic}}/\langle\sigma v\rangle_{\text{ID}}]$. In particular, Fig. 7 shows the two cases $\rho_\phi(T_{\text{BBN}}) = 0$ (left column) and $3 \times 10^{-2} \rho_{\text{BBN}}$ (right column), while Fig. 8 corresponds to $\rho_\phi(T_{\text{BBN}}) = 10^{-4} \rho_{\text{BBN}}$. In both figures we present our results for three values of the WIMP mass, $m_\chi = 1000$ GeV (top panels), 100 GeV (middle panels) and 10 GeV (bottom panels). The white regions of the parameter space have $\langle\sigma v\rangle_{\text{relic}}/\langle\sigma v\rangle_{\text{ID}} > 1$ and are disfavoured by indirect searches. In particular, the regions of parameters in dark blue are within one order of magnitude of the present sensitivity, $1/10 \lesssim \langle\sigma v\rangle_{\text{relic}}/\langle\sigma v\rangle_{\text{ID}} \lesssim 1$ and could be within the reach of future observations. As already pointed out, the results for negative values of $\dot{\phi}_{\text{BBN}}$ can be obtained by flipping the sign of γ . The plots in the left column of Fig. 7 show that the standard cosmological scenario is modified also for $\rho_\phi(T_{\text{BBN}}) = 0$, i.e. irrespective on the boundary conditions of the scalar field, as long as the $\tilde{\alpha}$ and γ parameters are non-vanishing. As confirmed by their top-down symmetry the results for $\rho_\phi(T_{\text{BBN}}) = 0$ do not depend on the sign of γ .

As already anticipated in the discussion of Section 4.1 the highest values of the enhancement factor A are found for $\tilde{\alpha}$ and γ positive and this is confirmed by the plots of Figs. 7 and 8, where the corresponding region is completely excluded for all three values of m_χ , unless $\dot{\phi}_{\text{BBN}} = 0$. As far as the latter case is concerned, a comparison between the plot for $m_\chi = 1$ TeV and $\dot{\phi}_{\text{BBN}} = 0$ in Fig. 7 and that of the corresponding enhancement factor A at $T = 50$ GeV (i.e. $m_\chi/20$) at the left-hand plot of Fig. 6 shows that, when $\tilde{\alpha}$ and γ are both positive, values of the enhancement factor as high as 10^5 do not drive $\langle\sigma v\rangle_{\text{gal}}$ beyond its upper bound. This shows that the value of $\langle\sigma v\rangle_{\text{gal}}$ does not scale directly with A and is a clear indication of the mitigating effect that the post-freeze-out WIMP annihilation process discussed in Section 3.1 can have on the relic density and that is expected when the temperature evolution of H is faster than in the standard case.

Another feature that is worth noticing at this stage is that the cases for $m_\chi = 10$ GeV and $\dot{\phi}_{\text{BBN}} \neq 0$ in Figs. 7 and 8 differ from those at higher values of m_χ , in that no allowed regions are found for $\tilde{\alpha} < 0$ and $\gamma > 0$. This is due to the fact that the plots of Figs. 7 and 8 depend on m_χ both through the shift of the decoupling temperature $T_f \sim m_\chi/20$ and because the experimental bounds on $\langle\sigma v\rangle_{\text{gal}}$ depend on the WIMP mass. In particular, as can be seen from Table 1, at low WIMP masses the present bounds on $\langle\sigma v\rangle_{\text{gal}}$ have already reached the standard value $3 \times 10^{-26} \text{ cm}^3 \text{ s}^{-1}$, i.e. they already exclude

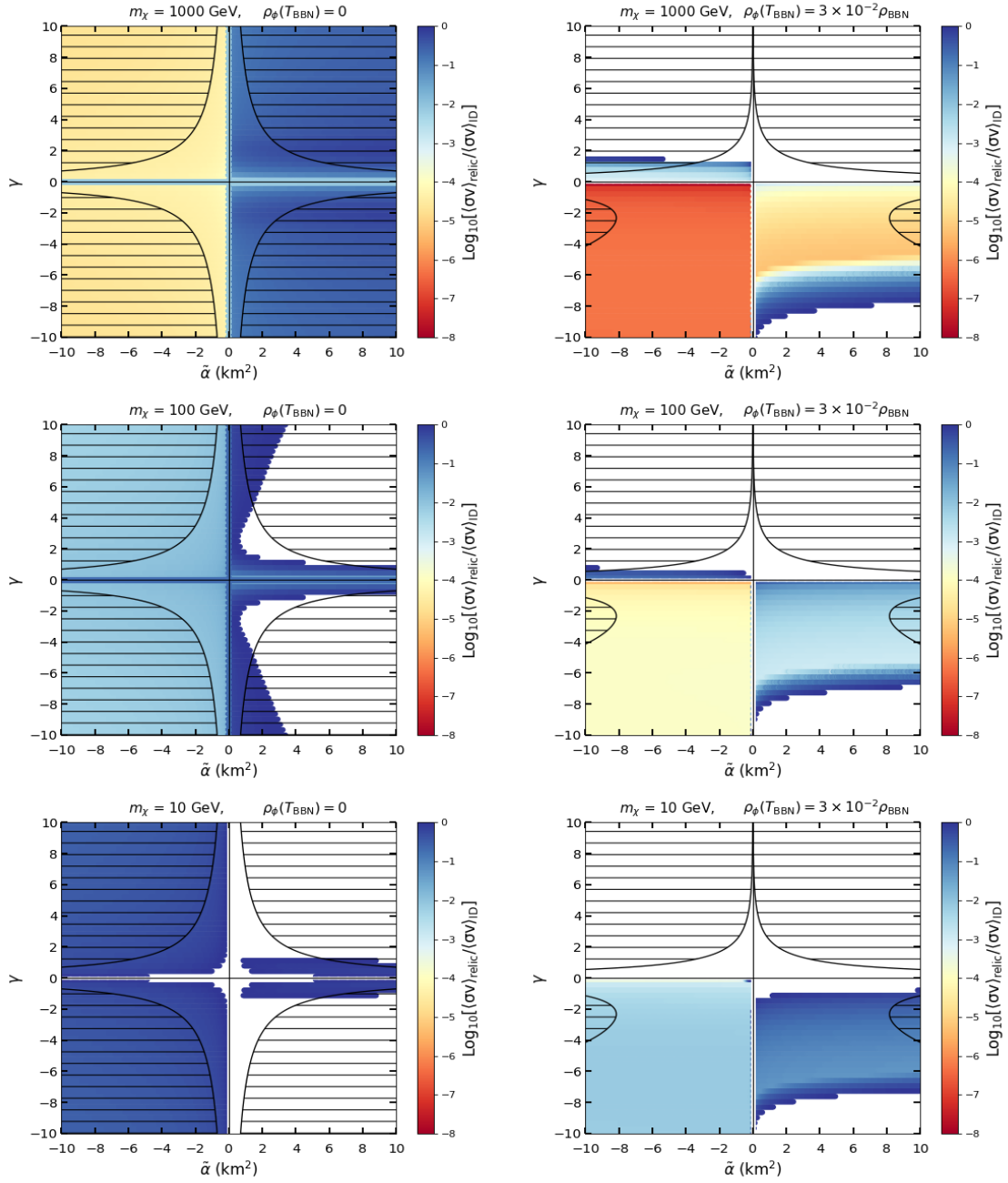


Figure 7. DEGB parameter space where the WIMP relic abundance corresponds to the observed one, i.e. $\Omega_\chi h^2 \simeq 0.12$. The color code refers to the ratio $\text{Log}_{10} [\langle \sigma v \rangle_{\text{relic}} / \langle \sigma v \rangle_{\text{ID}}]$. The white regions are excluded by WIMP indirect searches, while the hatched ones are ruled out by the detection of GW from compact binary mergers [38]. **Top:** $m_\chi = 1 \text{ TeV}$; **middle:** $m_\chi = 100 \text{ GeV}$; **bottom:** $m_\chi = 10 \text{ GeV}$. **Left column:** $\rho_\phi(T_{\text{BBN}}) = 0$; **Right column:** $\rho_\phi(T_{\text{BBN}}) = 3 \times 10^{-2} \rho_{\text{BBN}}$.

the standard scenario. In this case, at variance with what happens for higher WIMP masses, a modified cosmological scenario such as the dEGB model discussed in the present

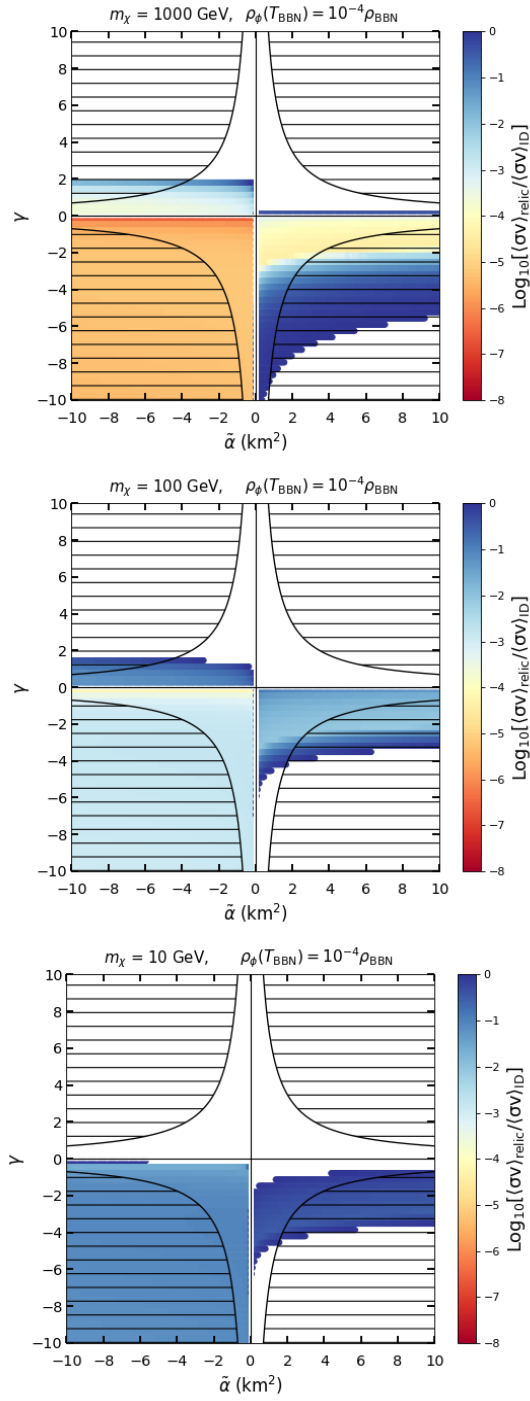


Figure 8. The same of Fig. 7 for $\rho_\phi(T_{\text{BBN}}) = 10^{-4}\rho_{\text{BBN}}$.

paper is actually *required* to reconcile the indirect detection bounds with the observed relic density.

We conclude by noticing that in Figs. 7 and 8 the hatched regions excluded by the late-time constraints from compact binary mergers discussed in Section 4.2.1 are nicely

complementary to those from WIMP indirect detection, with cases allowed/excluded by both bounds or excluded by only one of the two.

5 Conclusions

In the present paper we have applied the physics of WIMP decoupling to probe Cosmologies in a dilatonic Einstein Gauss-Bonnet (dEGB) scenario where the Gauss-Bonnet term is non-minimally coupled to a scalar field with vanishing potential. In particular, in such scenario standard cosmology is modified irrespective of the boundary conditions of the scalar field, as long as the non-minimal coupling is non-vanishing.

We have put constraints on the model parameters using the fact that in a modified cosmological scenario the WIMP annihilation cross section at freeze-out $\langle\sigma v\rangle_f$ required to predict the correct relic abundance is modified compared to the standard value $3\times 10^{-26}\text{ cm}^3\text{ s}^{-1}$ and this can drive the WIMP annihilation cross section in the halo of our Galaxy $\langle\sigma v\rangle_{\text{gal}}$ beyond the bounds from DM indirect detection searches, when $\langle\sigma v\rangle_f = \langle\sigma v\rangle_{\text{gal}}$. On the other hand, at low WIMP masses the present bounds on $\langle\sigma v\rangle_{\text{gal}}$ have already reached the standard value and already exclude the standard scenario, so that a modified cosmological scenario such as the one discussed in the present paper is required to reconcile the WIMP indirect detection bounds with the observed relic density. In our analysis we assumed WIMPs that annihilate to SM particles through an s-wave process.

At fixed $\langle\sigma v\rangle_f$ the relic abundance prediction grows with the enhancement factor A , given by the ratio between the Hubble constant in the dEGB scenario and its standard value. In particular, for a vanishing dEGB term the value of A is very large and incompatible with WIMP bounds unless $\dot{\phi}_{\text{BBN}}$ is much lower than the present constraints. On the other hand, for the class of solutions that comply with WIMP indirect detection bounds we found that the dEGB term plays a mitigating role on the scalar field (kination) dynamics, slowing down the speed of its evolution and reducing A . For such slow $\dot{\phi}$ solutions we observe that the corresponding boundary conditions at high temperature correspond asymptotically to an equation of state $w = -1/3$ and a vanishing deceleration parameter q . This implies that in this class of solutions the effect of dEGB at high T is to add an accelerating term that exactly cancels the deceleration predicted by GR. In this regime the density of the Universe is driven by $\rho_{\text{tot}} \simeq \rho_{\text{rad}} + \rho_{\text{GB}}$, with a large cancellation between ρ_{rad} and $\rho_{\text{GB}} < 0$.

The bounds that we found from WIMP indirect detection are nicely complementary to late-time constraints from compact binary mergers. This suggests that it could be interesting to use other Early Cosmology processes to probe the dEGB scenario. In particular, although from the phenomenological point of view the evolution of the Universe at temperatures much larger than the WIMP thermal decoupling are irrelevant to our analysis, it would be interesting to study the implications of the dEGB scenario on Inflation or on the evolution of density perturbations.

Acknowledgements

This research was supported by the National Research Foundation of Korea (NRF) funded by the Ministry of Education through the Center for Quantum Space Time (CQUeST) with grant number 2020R1A6A1A03047877, by the Ministry of Science and ICT with grant number 2021R1F1A1057119 (SS), NRF-2020R1F1A1075472 (BHL), NRF-2022R1I1A1A01067336 (WL), and NRF-2021R1A4A2001897 (AB). BHL thanks the hospitality of APCTP, where part of this work was done. LY thanks the YST Program of the APCTP.

A Comments on the semi-analytical solutions of the Friedmann equations

The evolution of the Friedmann equations in the dEGB scenario is highly non-linear, so a numerical discussion is mandatory in order to obtain reliable predictions. Anyway, using semi-analytical expression it is possible to get a qualitative insight on the class of solutions that are obtained numerically. In the following we wish to briefly clarify three specific issues: (i) the steep evolution of ρ_{GB} and its equation of state at T_{BBN} ; (ii) the back-reaction mechanism that stops the growth of $\dot{\phi}$ when the deceleration parameter changes sign; (iii) the asymptotic equation of state at high T when ρ_{ϕ} is subdominant.

A.1 Equation of state of the dEGB term at temperatures close to Big Bang Nucleosynthesis

The evolution of the scalar field and the scale factor is governed by Eqs. (4.2) and (4.4) which are reported here for convenience:

$$H^2 = \frac{\kappa}{3} (\rho_{\{\phi+\text{GB}\}} + \rho_{\text{rad}}) , \quad (\text{A.1})$$

$$\ddot{\phi} + 3H\dot{\phi} + V'_{\text{GB}} = 0 , \quad (\text{A.2})$$

where $V'_{\text{GB}} \equiv -f'R_{\text{GB}}^2 = -24f'H^2(\dot{H} + H^2) = 24\tilde{\alpha}\gamma e^{\gamma\phi} qH^4$. Near $T = T_{\text{BBN}}$ the Universe expansion is dominated by radiation $H \simeq \frac{1}{2t} \sim T^2$, while the GB term in the scalar field equation is negligible, so that $\dot{\phi} \sim t^{-3/2} \sim T^3$. With our choice of the initial condition $\dot{\phi}_{\text{BBN}} \geq 0$ and $\phi = 0$, the scalar field behavior is $\ddot{\phi} \leq 0$ and $\dot{\phi}$ as well as ϕ grow fast at higher temperature. In particular, the scalar energy density $\rho_{\phi} = \frac{1}{2}\dot{\phi}^2$ grows $\rho_{\phi} \sim T^6$, faster than $\rho_{\text{rad}} \sim T^4$ for higher T . Recall that the formal energy density for the Gauss-Bonnet $\rho_{\text{GB}} = -24f'\dot{\phi}H^3$ can be either positive or negative. In any case, neglecting in Eq. (2.10) the T dependence of $f'(\phi(T))$, its absolute magnitude will grow as $\rho_{\text{GB}} \sim T^9$, much faster than both $\rho_{\text{rad}} \sim T^4$ and $\rho_{\phi} \sim T^6$. Figs. 1 and 2 are consistent with this qualitative analysis. Moreover, using also (2.11) one obtains:

$$w_{\text{GB}} = \frac{p_{\text{GB}}}{\rho_{\text{GB}}} = -\frac{1}{3} \frac{d \ln(\dot{f}H^2)}{H dt} - \frac{2}{3} = \frac{1}{3} \frac{d \ln(\dot{f}H^2)}{d \ln T} - \frac{2}{3} , \quad (\text{A.3})$$

and so $w_{\text{GB}}(T_{\text{BBN}}) = 5/3$ (in good agreement with Fig. 4). Notice that the evolution of ρ_{GB} is coupled to that of ρ_{ϕ} , so $\rho_{\text{GB}} \neq T^{3(1+w_{\text{GB}})} = T^8$.

A.2 Back-reaction on the scalar field evolution from the change of sign of the deceleration parameter

As explained in A.1, in absence of the Gauss-Bonnet term the kinetic energy of the scalar field grows with temperature as $\rho_\phi \sim T^6$ and eventually dominates at higher temperature. In the allowed parameter space discussed in Section 4.2.2 the dEGB term is then instrumental in mitigating the growth of ρ_ϕ .

As explained in Section 4.1 the suppression of the growth of $\dot{\phi}$ is relatively easy to understand when close to T_{BBN} in Eq.(A.2) the two terms V'_{GB} and $3H\dot{\phi}$ have opposite sign, something that happens when $\rho_\phi(T_{\text{BBN}}) > 0$ and $\tilde{\alpha}\gamma < 0$. On the other hand, naively one may expect no suppression of the scalar field kinetic energy either when $\rho_\phi(T_{\text{BBN}}) = 0$ and $\tilde{\alpha} < 0$ (left-hand plot of Fig. 1) or when $\rho_\phi(T_{\text{BBN}}) > 0$ and the product $\tilde{\alpha}\gamma$ is positive (bottom-left plot of Fig. 2), since close to T_{BBN} in both cases V'_{GB} and $3H\dot{\phi}$ have the same sign. However, in Figs 1 and 2 one observes numerically a suppression of the growth of $\dot{\phi}$ also in such circumstances.

We wish here to provide a few comments on the non-linear back-reaction effect that is responsible of this behaviour. As already pointed out ρ_ϕ quickly dominates over ρ_{rad} above T_{BBN} . Soon after that also $|\rho_{\text{GB}}|$ reaches the level of ρ_ϕ , but since $\rho_{\text{GB}} < 0$ and the sum $\rho \sim \rho_\phi + \rho_{\text{GB}}$ must remain positive a large cancellation arises between ρ_ϕ and ρ_{GB} (this is observed both in Fig. 1 and 2). Since $|\rho_{\text{GB}}|$ tracks ρ_ϕ very closely one can assume $|\rho_{\text{GB}}| \sim \rho_\phi$. Setting $\dot{\phi} \sim T^\alpha$ and parameterizing the additional T dependence of f' as $f' \sim T^\xi$ (with $\xi > 0$ when $\gamma < 0$), one can find a relation between the two parameters α and ξ and the equation of state w that drives the total density, $\rho \sim T^{3(1+w)}$:

$$\rho_\phi \sim T^{2\alpha} \sim |\rho_{\text{GB}}| \sim T^{\alpha+\xi+\frac{9}{2}(1+w)} \rightarrow \alpha \sim \frac{9}{2}(1+w) + \xi. \quad (\text{A.4})$$

The same cancellation must happen in the pressure term, $p \sim p_\phi + p_{\text{GB}}$:

$$p = \rho_\phi + p_{\text{GB}} = \rho_\phi + \rho_{\text{GB}} + 8\frac{d(\dot{f}H^2)}{dt} - \frac{5}{3}\rho_{\text{GB}} \quad (\text{A.5})$$

so that also the term $8d(\dot{f}H^2)/dt = -8HTd(\dot{f}H^2)/dT$ must track closely $-5/3\rho_{\text{GB}} = 40\dot{f}H^3$, or $Td(\dot{f}H^2)/dT \sim 5\dot{f}H^2$. As a consequence:

$$\frac{d(\dot{f}H^2)}{\dot{f}H^2} \sim 5\frac{dT}{T} \rightarrow f'\dot{\phi}H^2 \sim T^{\xi+\alpha+3(1+w)} \sim T^5 \rightarrow \xi + \alpha + 3(1+w) = 5, \quad (\text{A.6})$$

and from the two relations (A.4) and (A.6) one gets:

$$\alpha = 3 - \frac{\xi}{5}, \quad w = -\frac{1}{3} - \frac{4}{15}\xi. \quad (\text{A.7})$$

The equation above shows that as $|\rho_{\text{GB}}|$ approaches ρ_ϕ the equation of state w turns smaller than $-1/3$, triggering a change of sign in the deceleration parameter $q = (1 + 3w)/2$. This implies that also V'_{GB} in the scalar field equation changes sign. Thanks to the exponential enhancement in f eventually V'_{GB} overcomes $3H\dot{\phi}$, flipping the sign of $\ddot{\phi}$ and stopping the growth of $\dot{\phi}$.

A.3 Equation of state at high temperature for subdominant kination energy

One can notice that in Figs. 3 and 4 whenever ρ_ϕ is subdominant at high temperature the corresponding equation of state of the Universe gets close to $w \sim -1/3$, i.e. $q = 0$. This implies that in this class of solutions the effect of dEGB is to add an accelerating term that exactly cancels the deceleration predicted by GR (notice that in our model $V = 0$).

This is an asymptotic solution of the Friedmann equation that can be verified by solving for \dot{H} in Eq. (4.3) and (4.4):

$$\dot{H} = -\frac{\kappa(8H^2 f'' \dot{\phi}^2 - 32H^3 f' \dot{\phi} + 192H^6 (f')^2 + p_{\text{rad}} + \rho_{\text{rad}} + \dot{\phi}^2)}{2(96\kappa(f')^2 H^4 + 8\kappa f' \dot{\phi} H + 1)}. \quad (\text{A.8})$$

In this specific scenario the density of the Universe is $\rho_{\text{tot}} \simeq \rho_{\text{rad}} + \rho_{\text{GB}} \gg \rho_\phi$, with ρ_{GB} closely tracking ρ_{rad} . We will write the terms in Eq. (A.8) by expressing f' , $f'' = \gamma f'$, $\dot{\phi}$ and κ in terms of $\rho_{\text{GB}} = -24f'H^3$, $\rho_\phi = \frac{1}{2}\dot{\phi}^2$ and using $\kappa = \frac{3H^2}{\rho_{\text{tot}}}$. Roughly speaking, f' is very large because it converts to ρ_{GB} , while $\dot{\phi}$ is very small because it converts to ρ_ϕ . Rewriting in terms of magnitude orders:

$$\dot{H} = -\frac{\kappa \left(192(f')^2 H^6 + 8f'' \dot{\phi}^2 H^2 + \frac{4}{3}(\rho_{\text{rad}} + \rho_{\text{GB}}) + \dot{\phi}^2 \right)}{2 \left(96\kappa(f')^2 H^4 + 8\kappa f' \dot{\phi} H + 1 \right)}. \quad (\text{A.9})$$

In this specific scenario the density of the Universe is $\rho_{\text{tot}} = \rho_{\text{rad}} + \rho_{\text{GB}} + \rho_\phi \simeq \rho_{\text{rad}} + \rho_{\text{GB}} \gg \rho_\phi$, with ρ_{GB} closely tracking ρ_{rad} . In other words, the hierarchies are ρ_{rad} and $|\rho_{\text{GB}}| \gg \rho_{\text{tot}} \simeq \rho_{\text{rad}} + \rho_{\text{GB}} \gg \rho_\phi$. Among the three independent terms ρ_{rad} , ρ_ϕ , ρ_{GB} (and $\rho_{\text{tot}} = \rho_{\text{rad}} + \rho_{\text{GB}} + \rho_\phi$) we can make two independent ratios, which we choose as $\left(\frac{\rho_\phi}{\rho_{\text{GB}}}\right)$ and $\left(\frac{\rho_{\text{tot}}}{\rho_{\text{GB}}}\right)$. These two ratios are very small numbers, allowing us to expand quantities in power series of these. The ratio of these two small numbers $\left(\frac{\rho_\phi}{\rho_{\text{tot}}}\right) \equiv r$ is also much smaller than 1 in our situation. Finally the ratio of radiation energy to ρ_{GB} is written as $\left(\frac{\rho_{\text{rad}}}{\rho_{\text{GB}}}\right) = -1 - \left(\frac{\rho_\phi}{\rho_{\text{GB}}}\right) + \left(\frac{\rho_{\text{tot}}}{\rho_{\text{GB}}}\right)$. This shows the tracking of ρ_{GB} to ρ_{rad} with the difference in terms of those two small independent ratios.

Using the following expressions:

$$\begin{aligned} 2 \times 96\kappa(f')^2 H^4 &= 2 \frac{96\kappa(f' \dot{\phi} H^3)^2}{\dot{\phi}^2 H^2} = \frac{1}{2} \left(\frac{\rho_{\text{GB}}}{\rho_{\text{tot}}}\right) \left(\frac{\rho_{\text{GB}}}{\rho_\phi}\right), \\ 2 \times 8\kappa f' \dot{\phi} H &= \frac{1}{2} \left(\frac{\rho_{\text{GB}}}{\rho_{\text{tot}}}\right) \left(\frac{\rho_{\text{GB}}}{\rho_\phi}\right) \left(-4 \left(\frac{\rho_\phi}{\rho_{\text{GB}}}\right)\right), \end{aligned} \quad (\text{A.10})$$

the denominator can be written as

$$\text{Denominator} = \frac{1}{2} \left(\frac{\rho_{\text{GB}}}{\rho_{\text{tot}}}\right) \left(\frac{\rho_{\text{GB}}}{\rho_\phi}\right) \left(1 - 4 \left(\frac{\rho_\phi}{\rho_{\text{GB}}}\right) + 4 \left(\frac{\rho_{\text{tot}}}{\rho_{\text{GB}}}\right) \left(\frac{\rho_\phi}{\rho_{\text{GB}}}\right)\right). \quad (\text{A.11})$$

In the numerator the first two terms are:

$$\begin{aligned} \kappa 192(f')^2 H^6 &= \frac{H^2}{2} \left(\frac{\rho_{\text{GB}}}{\rho_{\text{tot}}}\right) \left(\frac{\rho_{\text{GB}}}{\rho_\phi}\right), \\ 8\kappa f'' \dot{\phi}^2 H^2 &= \frac{H^2}{2} \left(\frac{\rho_{\text{GB}}}{\rho_{\text{tot}}}\right) \left(\frac{\rho_{\text{GB}}}{\rho_\phi}\right) \left(-2\gamma \sqrt{\frac{6r}{\kappa}} \left(\frac{\rho_\phi}{\rho_{\text{GB}}}\right)\right). \end{aligned} \quad (\text{A.12})$$

The remaining terms are:

$$\begin{aligned}
\frac{4}{3}\kappa(\rho_{\text{rad}} + \rho_{\text{GB}}) &= 4H^2 \left(\frac{\rho_{\text{GB}}}{\rho_{\text{tot}}} \right) \left(-1 + \left(\frac{\rho_{\text{tot}}}{\rho_{\text{GB}}} \right) - \left(\frac{\rho_{\phi}}{\rho_{\text{GB}}} \right) + 1 \right) \\
&= \frac{H^2}{2} \left(\frac{\rho_{\text{GB}}}{\rho_{\text{tot}}} \right) \left(\frac{\rho_{\text{GB}}}{\rho_{\phi}} \right) \left(8 \left(\frac{\rho_{\phi}}{\rho_{\text{GB}}} \right) \left(\frac{\rho_{\text{tot}}}{\rho_{\text{GB}}} \right) - 8 \left(\frac{\rho_{\phi}}{\rho_{\text{GB}}} \right)^2 \right), \\
\kappa\dot{\phi}^2 &= \frac{H^2}{2} \left(\frac{\rho_{\text{GB}}}{\rho_{\text{tot}}} \right) \left(\frac{\rho_{\text{GB}}}{\rho_{\phi}} \right) \left(12 \left(\frac{\rho_{\phi}}{\rho_{\text{GB}}} \right)^2 \right). \tag{A.13}
\end{aligned}$$

By summing Eqs. (A.12) and (A.12), the numerator becomes:

$$\frac{H^2}{2} \left(\frac{\rho_{\text{GB}}}{\rho_{\text{tot}}} \right) \left(\frac{\rho_{\text{GB}}}{\rho_{\phi}} \right) \left(1 - 2\gamma\sqrt{\frac{6r}{\kappa}} \left(\frac{\rho_{\phi}}{\rho_{\text{GB}}} \right) + 8 \left(\frac{\rho_{\phi}}{\rho_{\text{GB}}} \right) \left(\frac{\rho_{\text{tot}}}{\rho_{\text{GB}}} \right) + 4 \left(\frac{\rho_{\phi}}{\rho_{\text{GB}}} \right)^2 \right). \tag{A.14}$$

Finally, we get \dot{H} in Eq. (A.9) by combining Eqs. (A.11) and (A.14):

$$\dot{H} = -H^2 \frac{1 - 2\gamma\sqrt{\frac{6r}{\kappa}} \left(\frac{\rho_{\phi}}{\rho_{\text{GB}}} \right) + (8 + 4r) \left(\frac{\rho_{\phi}}{\rho_{\text{GB}}} \right) \left(\frac{\rho_{\text{tot}}}{\rho_{\text{GB}}} \right)}{1 - 4 \left(\frac{\rho_{\phi}}{\rho_{\text{GB}}} \right) + 4 \left(\frac{\rho_{\text{tot}}}{\rho_{\text{GB}}} \right) \left(\frac{\rho_{\phi}}{\rho_{\text{GB}}} \right)}. \tag{A.15}$$

Keeping the leading term in the expansion:

$$\frac{\dot{H}}{H^2} = -(1 + q) \simeq - \left(1 + \left(4 - 2\gamma\sqrt{\frac{6r}{\kappa}} \right) \left(\frac{\rho_{\phi}}{\rho_{\text{GB}}} \right) \right), \tag{A.16}$$

and finally, at leading order the deceleration is given by:

$$q \simeq \left(4 + 2\gamma\sqrt{\frac{6r}{\kappa}} \right) \left(\frac{\rho_{\phi}}{\rho_{\text{GB}}} \right) \simeq 4 \left(\frac{\rho_{\phi}}{\rho_{\text{GB}}} \right). \tag{A.17}$$

In the last equation we dropped the r -dependent term since $r \ll 1$ and $\kappa = 1$ in our setting. As a consequence, q is a small non-vanishing negative number. Indeed, from the plots of Fig. 2 one can see that numerically the parameter $|\rho_{\phi}/\rho_{\text{GB}}|$ can be extremely small in this regime. This implies that in this scenario the Universe at high temperature expands with a very tiny acceleration and equation of state $w \simeq -1/3$, eventually catching up Standard Cosmology and radiation dominance at much lower temperatures. Moreover, from Eq. (A.17) one has $q \times \rho_{\text{GB}}/\rho_{\phi} \rightarrow 4$, so that

$$\frac{V'_{\text{GB}}}{3H\dot{\phi}} = -\frac{1}{6}q \frac{\rho_{\text{GB}}}{\rho_{\phi}} \rightarrow -\frac{2}{3} \tag{A.18}$$

and in this regime the scalar field equation becomes:

$$\ddot{\phi} + H\dot{\phi} = 0, \tag{A.19}$$

that implies $\rho_{\phi} \simeq T^2$, as confirmed explicitly in the plots of Fig. 2 where ρ_{ϕ} is subdominant.

It is worth noticing that, while, as shown in Fig. 4, this implies that both ρ_{rad} and ρ_{GB} have separate equation of state $w = 1/3$, as explained above the equation of state for their combination $\rho_{\text{rad}} + \rho_{\text{GB}}$ is instead $-1/3$. This can be understood because the equation of state of the Universe $w = p/\rho$ is the result of a limit where both p and ρ have very large cancellations, i.e. $w \rightarrow 0/0$.

References

- [1] T. Clifton, P. G. Ferreira, A. Padilla and C. Skordis, *Modified Gravity and Cosmology*, *Phys. Rept.* **513** (2012) 1–189, [[1106.2476](#)].
- [2] S. Nojiri and S. D. Odintsov, *Unified cosmic history in modified gravity: from $F(R)$ theory to Lorentz non-invariant models*, *Phys. Rept.* **505** (2011) 59–144, [[1011.0544](#)].
- [3] C. M. Will, *The Confrontation between General Relativity and Experiment*, *Living Rev. Rel.* **17** (2014) 4, [[1403.7377](#)].
- [4] G. W. Horndeski, *Second-order scalar-tensor field equations in a four-dimensional space*, *Int. J. Theor. Phys.* **10** (1974) 363–384.
- [5] R. P. Woodard, *Ostrogradsky’s theorem on Hamiltonian instability*, *Scholarpedia* **10** (2015) 32243, [[1506.02210](#)].
- [6] S. Tsujikawa, *Quintessence: A Review*, *Class. Quant. Grav.* **30** (2013) 214003, [[1304.1961](#)].
- [7] T. Harko, F. S. N. Lobo and M. K. Mak, *Arbitrary scalar field and quintessence cosmological models*, *Eur. Phys. J. C* **74** (2014) 2784, [[1310.7167](#)].
- [8] M. Cicoli, S. De Alwis, A. Maharana, F. Muia and F. Quevedo, *De Sitter vs Quintessence in String Theory*, *Fortsch. Phys.* **67** (2019) 1800079, [[1808.08967](#)].
- [9] S. Bahamonde, C. G. Böhmmer, S. Carloni, E. J. Copeland, W. Fang and N. Tamanini, *Dynamical systems applied to cosmology: dark energy and modified gravity*, *Phys. Rept.* **775–777** (2018) 1–122, [[1712.03107](#)].
- [10] S. Alexander and E. McDonough, *Axion-Dilaton Destabilization and the Hubble Tension*, *Phys. Lett. B* **797** (2019) 134830, [[1904.08912](#)].
- [11] A. Banerjee, H. Cai, L. Heisenberg, E. O. Colgáin, M. M. Sheikh-Jabbari and T. Yang, *Hubble sinks in the low-redshift swampland*, *Phys. Rev. D* **103** (2021) L081305, [[2006.00244](#)].
- [12] S. D. Odintsov and V. K. Oikonomou, *The reconstruction of $f(\phi)R$ and mimetic gravity from viable slow-roll inflation*, *Nucl. Phys. B* **929** (2018) 79–112, [[1801.10529](#)].
- [13] S. Nojiri and S. D. Odintsov, *Introduction to modified gravity and gravitational alternative for dark energy*, *eConf* **C0602061** (2006) 06, [[hep-th/0601213](#)].
- [14] J.-c. Hwang and H. Noh, *Conserved cosmological structures in the one loop superstring effective action*, *Phys. Rev. D* **61** (2000) 043511, [[astro-ph/9909480](#)].
- [15] M. Satoh and J. Soda, *Higher Curvature Corrections to Primordial Fluctuations in Slow-roll Inflation*, *JCAP* **09** (2008) 019, [[0806.4594](#)].
- [16] B. Zwiebach, *Curvature Squared Terms and String Theories*, *Phys. Lett. B* **156** (1985) 315–317.
- [17] P. Kanti, N. E. Mavromatos, J. Rizos, K. Tamvakis and E. Winstanley, *Dilatonic black holes in higher curvature string gravity*, *Phys. Rev. D* **54** (1996) 5049–5058, [[hep-th/9511071](#)].
- [18] R.-G. Cai, *Gauss-Bonnet black holes in AdS spaces*, *Phys. Rev. D* **65** (2002) 084014, [[hep-th/0109133](#)].
- [19] Z.-K. Guo and D. J. Schwarz, *Slow-roll inflation with a Gauss-Bonnet correction*, *Phys. Rev. D* **81** (2010) 123520, [[1001.1897](#)].
- [20] S. Koh, B.-H. Lee, W. Lee and G. Tumurtushaa, *Observational constraints on slow-roll inflation coupled to a Gauss-Bonnet term*, *Phys. Rev. D* **90** (2014) 063527, [[1404.6096](#)].

- [21] G. Cognola, E. Elizalde, S. Nojiri, S. Odintsov and S. Zerbini, *String-inspired Gauss-Bonnet gravity reconstructed from the universe expansion history and yielding the transition from matter dominance to dark energy*, *Phys. Rev. D* **75** (2007) 086002, [[hep-th/0611198](#)].
- [22] W.-K. Ahn, B. Gwak, B.-H. Lee and W. Lee, *Instability of Black Holes with a Gauss-Bonnet Term*, *Eur. Phys. J. C* **75** (2015) 372, [[1412.4189](#)].
- [23] S. Khimphun, B.-H. Lee and W. Lee, *Phase transition for black holes in dilatonic Einstein-Gauss-Bonnet theory of gravitation*, *Phys. Rev. D* **94** (2016) 104067, [[1605.07377](#)].
- [24] B.-H. Lee, W. Lee and D. Ro, *Fubini instantons in Dilatonic Einstein-Gauss-Bonnet theory of gravitation*, *Phys. Lett. B* **762** (2016) 535–542, [[1607.01125](#)].
- [25] G. Antoniou, A. Bakopoulos and P. Kanti, *Evasion of No-Hair Theorems and Novel Black-Hole Solutions in Gauss-Bonnet Theories*, *Phys. Rev. Lett.* **120** (2018) 131102, [[1711.03390](#)].
- [26] D. D. Doneva and S. S. Yazadjiev, *New Gauss-Bonnet Black Holes with Curvature-Induced Scalarization in Extended Scalar-Tensor Theories*, *Phys. Rev. Lett.* **120** (2018) 131103, [[1711.01187](#)].
- [27] H. O. Silva, J. Sakstein, L. Gualtieri, T. P. Sotiriou and E. Berti, *Spontaneous scalarization of black holes and compact stars from a Gauss-Bonnet coupling*, *Phys. Rev. Lett.* **120** (2018) 131104, [[1711.02080](#)].
- [28] Y. S. Myung and D.-C. Zou, *Gregory-Laflamme instability of black hole in Einstein-scalar-Gauss-Bonnet theories*, *Phys. Rev. D* **98** (2018) 024030, [[1805.05023](#)].
- [29] B.-H. Lee, W. Lee and D. Ro, *Expanded evasion of the black hole no-hair theorem in dilatonic Einstein-Gauss-Bonnet theory*, *Phys. Rev. D* **99** (2019) 024002, [[1809.05653](#)].
- [30] X. Y. Chew, G. Tumurtushaa and D.-h. Yeom, *Euclidean wormholes in Gauss-Bonnet-dilaton gravity*, *Phys. Dark Univ.* **32** (2021) 100811, [[2006.04344](#)].
- [31] B.-H. Lee, H. Lee and W. Lee, *Hairy black holes in dilatonic Einstein-Gauss-Bonnet theory*, in *17th Italian-Korean Symposium on Relativistic Astrophysics*, 11, 2021, [[2111.13380](#)].
- [32] S. Kawai and J. Kim, *Primordial black holes from Gauss-Bonnet-corrected single field inflation*, *Phys. Rev. D* **104** (2021) 083545, [[2108.01340](#)].
- [33] A. Papageorgiou, C. Park and M. Park, *Rectifying No-Hair Theorems in Gauss-Bonnet theory*, [[2205.00907](#)].
- [34] R. Nair, S. Perkins, H. O. Silva and N. Yunes, *Fundamental Physics Implications for Higher-Curvature Theories from Binary Black Hole Signals in the LIGO-Virgo Catalog GWTC-1*, *Phys. Rev. Lett.* **123** (2019) 191101, [[1905.00870](#)].
- [35] M. Okounkova, *Numerical relativity simulation of GW150914 in Einstein dilaton Gauss-Bonnet gravity*, *Phys. Rev. D* **102** (2020) 084046, [[2001.03571](#)].
- [36] H.-T. Wang, S.-P. Tang, P.-C. Li, M.-Z. Han and Y.-Z. Fan, *Tight constraints on Einstein-dilation-Gauss-Bonnet gravity from GW190412 and GW190814*, *Phys. Rev. D* **104** (2021) 024015.
- [37] S. E. Perkins, R. Nair, H. O. Silva and N. Yunes, *Improved gravitational-wave constraints on higher-order curvature theories of gravity*, *Phys. Rev. D* **104** (2021) 024060, [[2104.11189](#)].
- [38] Z. Lyu, N. Jiang and K. Yagi, *Constraints on Einstein-dilation-Gauss-Bonnet gravity from*

- black hole-neutron star gravitational wave events, *Phys. Rev. D* **105** (2022) 064001, [[2201.02543](#)].
- [39] M. Kusakabe, S. Koh, K. S. Kim and M.-K. Cheoun, *Constraints on modified Gauss-Bonnet gravity during big bang nucleosynthesis*, *Phys. Rev. D* **93** (2016) 043511, [[1507.05565](#)].
- [40] P. Asimakis, S. Basilakos, N. E. Mavromatos and E. N. Saridakis, *Big bang nucleosynthesis constraints on higher-order modified gravities*, *Phys. Rev. D* **105** (2022) 084010, [[2112.10863](#)].
- [41] L. Amendola, C. Charmousis and S. C. Davis, *Constraints on Gauss-Bonnet gravity in dark energy cosmologies*, *JCAP* **12** (2006) 020, [[hep-th/0506137](#)].
- [42] P. Salati, *Quintessence and the relic density of neutralinos*, *Phys. Lett. B* **571** (2003) 121–131, [[astro-ph/0207396](#)].
- [43] F. Rosati, *Quintessential enhancement of dark matter abundance*, *Phys. Lett. B* **570** (2003) 5–10, [[hep-ph/0302159](#)].
- [44] J. U. Kang and G. Panotopoulos, *Big-Bang Nucleosynthesis and neutralino dark matter in modified gravity*, *Phys. Lett. B* **677** (2009) 6–11, [[0806.1493](#)].
- [45] S. Capozziello, M. De Laurentis and G. Lambiase, *Cosmic relic abundance and $f(R)$ gravity*, *Phys. Lett. B* **715** (2012) 1–8, [[1201.2071](#)].
- [46] S. Capozziello, V. Galluzzi, G. Lambiase and L. Pizza, *Cosmological evolution of thermal relic particles in $f(R)$ gravity*, *Phys. Rev. D* **92** (2015) 084006, [[1507.06835](#)].
- [47] M. T. Meehan and I. B. Whittingham, *Dark matter relic density in scalar-tensor gravity revisited*, *JCAP* **12** (2015) 011, [[1508.05174](#)].
- [48] G. Lambiase, *$f(R)$ cosmology and dark matter*, *PoS DSU2015* (2016) 012.
- [49] F. D’Eramo, N. Fernandez and S. Profumo, *When the Universe Expands Too Fast: Relentless Dark Matter*, *JCAP* **05** (2017) 012, [[1703.04793](#)].
- [50] M. Schelke, R. Catena, N. Fornengo, A. Masiero and M. Pietroni, *Constraining pre Big-Bang-Nucleosynthesis Expansion using Cosmic Antiprotons*, *Phys. Rev. D* **74** (2006) 083505, [[hep-ph/0605287](#)].
- [51] F. Donato, N. Fornengo and M. Schelke, *Additional bounds on the pre big-bang-nucleosynthesis expansion by means of gamma-rays from the galactic center*, *JCAP* **03** (2007) 021, [[hep-ph/0612374](#)].
- [52] W. Buchmuller, R. D. Peccei and T. Yanagida, *Leptogenesis as the origin of matter*, *Ann. Rev. Nucl. Part. Sci.* **55** (2005) 311–355, [[hep-ph/0502169](#)].
- [53] S. Kawai and J. Kim, *Gauss-Bonnet Chern-Simons gravitational wave leptogenesis*, *Phys. Lett. B* **789** (2019) 145–149, [[1702.07689](#)].
- [54] D. G. Boulware and S. Deser, *String Generated Gravity Models*, *Phys. Rev. Lett.* **55** (1985) 2656.
- [55] S.-M. Choi, H. M. Lee and M.-S. Seo, *Cosmic abundances of SIMP dark matter*, *JHEP* **04** (2017) 154, [[1702.07860](#)].
- [56] G. Steigman, B. Dasgupta and J. F. Beacom, *Precise Relic WIMP Abundance and its Impact on Searches for Dark Matter Annihilation*, *Phys. Rev. D* **86** (2012) 023506, [[1204.3622](#)].

- [57] AMS collaboration, M. Aguilar et al., *Electron and Positron Fluxes in Primary Cosmic Rays Measured with the Alpha Magnetic Spectrometer on the International Space Station*, *Phys. Rev. Lett.* **113** (2014) 121102.
- [58] AMS collaboration, M. Aguilar et al., *Towards Understanding the Origin of Cosmic-Ray Positrons*, *Phys. Rev. Lett.* **122** (2019) 041102.
- [59] L. A. Cavasonza, H. Gast, M. Krämer, M. Pellen and S. Schael, *Constraints on leptophilic dark matter from the ams-02 experiment*, *The Astrophysical Journal* **839** (apr, 2017) 36.
- [60] FERMI-LAT collaboration, M. Ackermann et al., *The Fermi Galactic Center GeV Excess and Implications for Dark Matter*, *Astrophys. J.* **840** (2017) 43, [1704.03910].
- [61] FERMI-LAT, DES collaboration, A. Albert et al., *Searching for Dark Matter Annihilation in Recently Discovered Milky Way Satellites with Fermi-LAT*, *Astrophys. J.* **834** (2017) 110, [1611.03184].
- [62] T. R. Slatyer, *Indirect dark matter signatures in the cosmic dark ages. I. Generalizing the bound on s-wave dark matter annihilation from Planck results*, *Phys. Rev. D* **93** (2016) 023527, [1506.03811].
- [63] M. Cirelli, G. Corcella, A. Hektor, G. Hutsi, M. Kadastik, P. Panci et al., *PPPC 4 DM ID: A Poor Particle Physicist Cookbook for Dark Matter Indirect Detection*, *JCAP* **03** (2011) 051, [1012.4515].
- [64] R. K. Leane, T. R. Slatyer, J. F. Beacom and K. C. Y. Ng, *GeV-scale thermal wimps: Not even slightly ruled out*, *Phys. Rev. D* **98** (Jul, 2018) 023016.
- [65] PLANCK collaboration, N. Aghanim et al., *Planck 2018 results. VI. Cosmological parameters*, *Astron. Astrophys.* **641** (2020) A6, [1807.06209].
- [66] T. P. Sotiriou and E. Barausse, *Post-Newtonian expansion for Gauss-Bonnet gravity*, *Phys. Rev. D* **75** (2007) 084007, [gr-qc/0612065].
- [67] K. Yagi, L. C. Stein and N. Yunes, *Challenging the Presence of Scalar Charge and Dipolar Radiation in Binary Pulsars*, *Phys. Rev. D* **93** (2016) 024010, [1510.02152].
- [68] K. Yagi, L. C. Stein, N. Yunes and T. Tanaka, *Post-Newtonian, Quasi-Circular Binary Inspirals in Quadratic Modified Gravity*, *Phys. Rev. D* **85** (2012) 064022, [1110.5950].
- [69] H. Witek, L. Gualtieri, P. Pani and T. P. Sotiriou, *Black holes and binary mergers in scalar Gauss-Bonnet gravity: scalar field dynamics*, *Phys. Rev. D* **99** (2019) 064035, [1810.05177].
- [70] J. L. Blázquez-Salcedo, C. F. B. Macedo, V. Cardoso, V. Ferrari, L. Gualtieri, F. S. Khoo et al., *Perturbed black holes in Einstein-dilaton-Gauss-Bonnet gravity: Stability, ringdown, and gravitational-wave emission*, *Phys. Rev. D* **94** (2016) 104024, [1609.01286].
- [71] LIGO SCIENTIFIC, VIRGO collaboration, B. P. Abbott et al., *GWTC-1: A Gravitational-Wave Transient Catalog of Compact Binary Mergers Observed by LIGO and Virgo during the First and Second Observing Runs*, *Phys. Rev. X* **9** (2019) 031040, [1811.12907].